Title

A longitudinal MRI and TSPO PET-based investigation of brain region-specific neuroprotection by diazepam versus midazolam following organophosphate-induced seizures

Authors

Hobson, Brad A

Rowland, Douglas J

Dou, Yimeng

et al.

Publication Date

2024-06-01

DOI

10.1016/j.neuropharm.2024.109918

Neuropharmacology 251 (2024) 109918

Contents lists available at ScienceDirect

Neuropharmacology

journal homepage: www.elsevier.com/locate/neuropharm

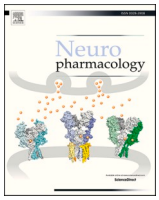

A longitudinal MRI and TSPO PET-based investigation of brain region-specific neuroprotection by diazepam *versus* midazolam following organophosphate-induced seizures

Brad A. Hobson [a,b], Douglas J. Rowland [b], Yimeng Dou [a], Naomi Saito [c], Zachary T. Harmany [b], Donald A. Bruun [a], Danielle J. Harvey [c], Abhijit J. Chaudhari [b,d], Joel R. Garbow [e], Pamela J. Lein [a,*]

[a] *Department of Molecular Biosciences, University of California, Davis, School of Veterinary Medicine, Davis, CA 95616, USA*
[b] *Center for Molecular and Genomic Imaging, University of California, Davis, College of Engineering, Davis, CA 95616, USA*
[c] *Department of Public Health Sciences, University of California, Davis, School of Medicine, California 95616, USA*
[d] *Department of Radiology, University of California, Davis, School of Medicine, California 95817, USA*
[e] *Biomedical Magnetic Resonance Center, Mallinckrodt Institute of Radiology, School of Medicine, Washington University in St. Louis, St. Louis, Missouri, 63110, USA*

ARTICLE INFO

Handling Editor: Bruno Frenguelli

Keywords:
Benzodiazepines
Diisopropylfluorophosphate
In vivo imaging
Neuroinflammation
Rat
Status epilepticus

ABSTRACT

Acute poisoning with organophosphorus cholinesterase inhibitors (OPs), such as OP nerve agents and pesticides, can cause life threatening cholinergic crisis and *status epilepticus (SE)*. Survivors often experience significant morbidity, including brain injury, acquired epilepsy, and cognitive deficits. Current medical countermeasures for acute OP poisoning include a benzodiazepine to mitigate seizures. Diazepam was long the benzodiazepine included in autoinjectors used to treat OP-induced seizures, but it is now being replaced in many guidelines by midazolam, which terminates seizures more quickly, particularly when administered intramuscularly. While a direct correlation between seizure duration and the extent of brain injury has been widely reported, there are limited data comparing the neuroprotective efficacy of diazepam *versus* midazolam following acute OP intoxication. To address this data gap, we used non-invasive imaging techniques to longitudinally quantify neuropathology in a rat model of acute intoxication with the OP diisopropylfluorophosphate (DFP) with and without post-exposure intervention with diazepam or midazolam. Magnetic resonance imaging (MRI) was used to monitor neuropathology and brain atrophy, while positron emission tomography (PET) with a radiotracer targeting translocator protein (TSPO) was utilized to assess neuroinflammation. Animals were scanned at 3, 7, 28, 65, 91, and 168 days post-DFP and imaging metrics were quantitated for the hippocampus, amygdala, piriform cortex, thalamus, cerebral cortex and lateral ventricles. In the DFP-intoxicated rat, neuroinflammation persisted for the duration of the study coincident with progressive atrophy and ongoing tissue remodeling. Benzodiazepines attenuated neuropathology in a region-dependent manner, but neither benzodiazepine was effective in attenuating long-term neuroinflammation as detected by TSPO PET. Diffusion MRI and TSPO PET metrics were highly correlated with seizure severity, and early MRI and PET metrics were positively correlated with long-term brain atrophy. Collectively, these results suggest that anti-seizure therapy alone is insufficient to prevent long-lasting neuroinflammation and tissue remodeling.

1. Introduction

Acute poisoning with organophosphorus cholinesterase inhibitors (OPs), including OP nerve agents and pesticides, due to occupational, intentional, and terrorism-related exposures is the cause of hundreds of thousands of deaths each year (reviewed in Brooks et al., 2018; Mew et al., 2017). The organophosphate form of these agents, which may be the parent compound itself, as is the case for many OP nerve agents, or

* Corresponding author. Molecular Biosciences, UC Davis School of Veterinary Medicine, 1089 Veterinary Medicine Drive, Davis, CA, 95616, USA.
E-mail addresses: bahobson@ucdavis.edu (B.A. Hobson), djrowland@ucdavis.edu (D.J. Rowland), ydou8@wisc.edu (Y. Dou), nhsaito@ucdavis.edu (N. Saito), zharmany@gmail.com (Z.T. Harmany), dabruun@ucdavis.edu (D.A. Bruun), djharvey@ucdavis.edu (D.J. Harvey), ajchaudhari@ucdavis.edu (A.J. Chaudhari), garbow@wustl.edu (J.R. Garbow), pjlein@ucdavis.edu (P.J. Lein).

https://doi.org/10.1016/j.neuropharm.2024.109918
Received 29 November 2023; Received in revised form 1 March 2024; Accepted 13 March 2024
Available online 24 March 2024

may be a metabolite, which is more often true of the OP pesticides, can cause acute toxicity by inhibiting acetylcholinesterase (AChE). Acute inhibition of AChE by > 70% causes prolonged activation of cholinergic signaling followed by subsequent overactivation of glutamatergic signaling. These molecular effects trigger life-threatening autonomic dysfunction, respiratory distress, and *status epilepticus* (SE) (Chen, 2012). Individuals who survive acute OP poisoning often suffer significant morbidity in the form of cognitive deficits, structural changes in the brain, and electrophysiological abnormalities (reviewed in Figueiredo et al., 2018; Jett et al., 2020; Savage et al., 1988). Animal models of acute OP intoxication have been shown to recapitulate these neurologic sequelae (reviewed in Andrew and Lein, 2021; Guignet et al., 2020; Pereira et al., 2014), exhibiting ongoing neuropathology, neuroinflammation, brain atrophy, spontaneous recurrent seizures and cognitive deficits that persist up to months after OP exposure (reviewed in Aroniadou-Anderjaska et al., 2016; Reddy et al., 2020; Supasai et al., 2020).

Current medical countermeasures against OP poisoning include atropine to attenuate parasympathomimetic effects, oximes to reactivate AChE and a benzodiazepine to reduce seizure activity (Eddleston et al., 2008; reviewed in Newmark, 2004). These therapeutics reduce mortality but do not adequately terminate seizure activity or attenuate adverse neurologic sequelae unless administered within minutes of OP poisoning. However, in mass casualty events or suicides, administration of therapeutics may be significantly delayed (Arca et al., 2020; Heemskerk et al., 2022; Hill et al., 2017; Kapur et al., 2019; Kim et al., 2018; Kirschenbaum et al., 2005; Pfenninger et al., 2020; Power et al., 2016; Vardell, 2012). This is problematic because extended SE in humans can become refractory to therapy (reviewed in Vossler et al., 2020) and OP-induced SE in monkeys (Lallement et al., 1998), rats (Apland et al., 2014; Shih et al., 1999), and guinea pigs (McDonough et al., 2010) can rapidly become refractory to benzodiazepines, prolonging seizure duration and increasing morbidity and mortality (Shih et al., 2003; Silbergleit et al., 2011; Towne, 2007). Midazolam (MDZ) has begun replacing the previously recommended benzodiazepine, diazepam (DZP), for the management of OP-induced SE, in large part because MDZ terminates seizures more quickly in rats (Krutak-Krol and Domino, 1985), mice (Raines et al., 1990), guinea pigs (McDonough et al., 1999) and humans (reviewed in Brigo et al., 2015), and it is easier to administer in the field (Silbergleit et al., 2011). However, there is limited information comparing the efficacy of DZP *versus* MDZ in mitigating the development and progression of long-term neuropathology, particularly when administered at delayed times after acute OP intoxication (Reddy et al., 2021; Supasai et al., 2020).

Evaluating long-term neuroprotection following acute OP intoxication in animal models can be challenging due to not only inter-animal variability in response to acute OP intoxication and/or treatment (Gage et al., 2021; Gonzalez et al., 2020; Pereira et al., 2014; Wu et al., 2018a), but also regional variation in the pattern and progression of injury within the brain (Hobson et al., 2017a; Scholl et al., 2018; Supasai et al., 2020). It is unclear what time point after therapeutic intervention, if any, is representative of long-term outcomes or the resolution of pathological processes. Non-invasive medical imaging techniques have been highly successful in identifying neuropathology in preclinical models of acute OP intoxication (Bar-Klein et al. 2016, 2017; Bhagat et al. 2001, 2005; Carpentier et al., 2008; Gullapalli et al., 2010; Hobson et al. 2017a, 2017b, 2019; Reddy et al., 2020; Rosman et al., 2012; Shrot et al., 2012; Testylier et al., 2007). Techniques such as magnetic resonance imaging (MRI), positron emission tomography (PET), and X-ray computerized tomography (CT) are well suited for long-term assessment of neurological sequela and therapeutic response since quantitative outcome measures can be monitored longitudinally within individual animals. To date, numerous MRI-based studies using a variety of contrast mechanisms including, but not limited to, T_2 in guinea pigs (Gullapalli et al., 2010), and diffusion (Hobson et al., 2017b), spectroscopy (Shrot et al., 2012) and extrinsic-contrast-enhancement (Bar-Klein et al., 2017) in rats have been used to characterize lesions following acute OP intoxication. However, investigations have been heavily weighted toward time points within the first week post-exposure (Bhagat et al. 2001, 2005; Carpentier et al., 2008; Gullapalli et al., 2010; Hobson et al., 2017a; Shrot et al. 2012, 2015; Testylier et al., 2007). Fewer imaging studies have assessed the impact of acute OP intoxication on the brain at one month post-intoxication (Bar-Klein et al. 2016, 2017; Hobson et al., 2017b) and beyond (Reddy et al., 2020; Rosman et al., 2012). Results from those studies demonstrate ongoing pathology and unresolved lesions supported by histological and behavioral data (Guignet et al., 2020; Supasai et al., 2020). Collectively, these reports suggest that while current standard-of-care can attenuate initial neuropathology and inflammation in the first few weeks post-exposure, this attenuation is not necessarily predictive of successful mitigation of adverse neurological outcomes at post-exposure times greater than one month (Supasai et al., 2020).

Brain atrophy, characterized by enlarged ventricular structures and decreased regional brain volumes, is one of the most consistent radiological findings in preclinical models of OP intoxication including guinea pigs (Gullapalli et al., 2010) and rats (Hobson et al., 2017b; Reddy et al., 2020; Rosman et al., 2012), and has additionally been observed in human clinical case reports (Yamasue et al., 2007). Atrophy, also a common finding in preclinical seizure models (Jupp et al., 2012; Yankam Njiwa et al., 2017) and epileptic patients (Bernhardt et al., 2009), is widely believed to result from progressive loss of neuronal tissue (Polli et al., 2014). Volumetric analysis of brain regions and cerebral spinal fluid (CSF) is, therefore, increasingly used to evaluate the success of medical interventions (Gullapalli et al., 2010; Hobson et al., 2017b; Reddy et al., 2020; Suleymanova et al., 2014). Quantitative T_2 and diffusion metrics from MRI of lesions in preclinical models of acute OP intoxication have been associated with necrosis, edema (Testylier et al., 2007), inflammation (Hobson et al., 2017b), and tissue remodeling such as scarring or mineralization (Siso et al., 2017).

The objective of the present study is to compare the neuroprotective efficacy of DZP and MDZ in a single cohort of rats acutely intoxicated with the OP diisopropylfluorophosphate (DFP) using longitudinal T_2-weighted and diffusion MRI as readouts of neuropathology and brain atrophy, and TSPO PET with the [^{18}F]PBR111 radiotracer as a specific readout of neuroinflammation (reviewed in Werry et al., 2019). DFP shares structural similarities to the OP nerve agents, sarin and soman, and produces similar robust neuropathology (Brewer et al., 2013; Kuruba et al., 2018; Siso et al., 2017), neuroinflammation (Flannery et al., 2016; Hobson et al., 2019; Kuruba et al., 2018), brain atrophy (Hobson et al., 2017a) and clinically-relevant behavioral deficits (Guignet et al., 2020). This longitudinal study seeks to extend the preclinical characterization of progressive neuropathology caused by acute OP intoxication by monitoring previously established imaging metrics (Hobson et al. 2017a, 2017b, 2019; Reddy et al., 2020) across multiple brain regions in the days, weeks, and months out to 168 days (approximately 6 months) post-intoxication in individual animals intoxicated with DFP and administered either vehicle, MDZ or DZP at a delayed time (40 min) post-exposure. Further, the utility of a battery of multimodal imaging measures for quantifying therapeutic response is evaluated over a range of times post-exposure, and the ability of early imaging metrics to predict long-term brain atrophy is evaluated.

2. Materials and methods

2.1. Study approval

This study followed protocols approved by the UC Davis Institutional Animal Care and Use Committee (IACUC protocol number 21954) and used facilities fully accredited by the Association for Assessment and Accreditation of Laboratory Animal Care (AAALAC) International. All experiments were performed in accordance with the ARRIVE guidelines and the National Institute of Health (NIH) Guide for The Care and Use of

Laboratory Animals (NIH publication No. 8023, revised 1978).

2.2. Animal husbandry and dosing paradigm

Adult male Sprague Dawley rats (250–280g; Charles River Laboratories, Hollister, CA) were individually housed under controlled environmental conditions (22 ± 2 °C, 40–50% humidity) with a normal 12 h light/dark cycle in facilities fully accredited by the AAALAC. Food and water were provided *ad libitum*.

On the day of injections, animals were randomized into vehicle (VEH) or DFP-exposed groups using a random number generator. An overview of the DFP exposure paradigm is provided in Fig. 1A. DFP (Sigma Chemical Company, St Louis, MO, USA; purity = 90 ± 7% determined as previously described (Gao et al., 2016)) was administered to rats at 4 mg/kg in a total volume of 300 μl via subcutaneous (sc) injection between the shoulder blades. DFP was diluted immediately prior to injection with sterile, ice-cold phosphate buffered saline (PBS, 3.6 mM Na_2HPO_4, 1.4 mM NaH_2PO_4, 150 mM NaCl; pH 7.2) (Deshpande et al., 2010). VEH control animals were injected sc with an equal volume (300 μl) of ice-cold PBS in place of DFP. All rats additionally received the following: pyridostigmine bromide (0.1 mg/kg; TCI America, Portland, USA; >98% purity) injected im to the inner thigh 30 min prior to DFP administration, and a combined im injection to the alternate inner thigh of 2.0 mg/kg atropine sulfate (Sigma; >97% purity) and 25 mg/kg pralidoxime (2-PAM, Sigma; >99% purity) in saline 1 min after administration of DFP or vehicle. These agents significantly reduced mortality in the rat model of acute DFP intoxication (Bruun et al., 2019). Additionally, both atropine and 2-PAM are included in the autoinjectors used as the standard of care to treat humans acutely intoxicated with OPs (reviewed in Newmark, 2019). At 40 min post-exposure, DFP-intoxicated animals that exhibited consecutive seizure behavior scores ≥3 (seizure behavior scoring is described in the next paragraph) were randomized into one of three treatment groups: saline (0.9% NaCl; referred to hereafter as the DFP group), midazolam at 0.73 mg/kg im (USP grade; Hospira Inc., Lake Forest, IL, USA; DFP + MDZ group) or diazepam at 5.0 mg/kg ip (USP grade; Hospira Inc., ; DFP + DZP group) using a random number generator. Due to DZP's very poor bioavailability when administered im (Reddy and Reddy, 2015; Ulu et al., 2016), DZP was administered ip at a dose shown to reach therapeutic concentrations in the brain (Supasai et al., 2020; Ulu et al., 2016). The dose of MDZ was based on allometric scaling (Nair and Jacob, 2016) of a single 10 mg autoinjector provided in the ChemPack kit for treating acute OP intoxication in humans. We previously demonstrated that administration of DZP and MDZ via these routes and at these doses resulted in higher brain concentrations of MDZ than DZP at 10 min post-exposure, but comparable concentrations at all other time points out to 4 h in both brain and plasma (Supasai et al., 2020). Vehicle control animals (VEH) were injected with saline vehicle control (0.9% NaCl). At 4 h post-exposure, animals were injected sc with 10 ml 5% dextrose (w/v) in 0.9% (w/v) isotonic saline (Baxter International, Deerfield, IL, USA) to replace lost fluids and calories, and returned to their home cages. In addition to standard chow, animals were provided soft food for the following week.

The severity of seizure behavior was assessed using a previously described (Deshpande et al., 2010) five-point scale: 0, no signs or symptoms; 1, salivation, urination, lacrimation and/or defecation (SLUD); 2, muscle fasciculations and tremors; 3, forelimbs clonus; 4, rearing and hindlimb clonus; 5, rearing with falling and loss of righting reflex. Seizure behavior was scored at 5-min intervals, from 0 to 120 min post-DFP intoxication, and at 20-min intervals from 120 to 240 min post-DFP. Following the administration of MDZ, DZP or vehicle (e.g., shortly after the 40-min mark), scoring was performed by an observer blinded to treatment group. Repeated scores of three and above on this scale have been shown previously to correspond to electrographic SE, defined as sustained electrographic seizure activity lasting longer than 5 min, in a preclinical model of acute DFP intoxication (Guignet et al., 2020; Pouliot et al., 2016).

A total of 101 animals from ten separate injection cohorts were advanced into the *in vivo* imaging study (n = 7–11 animals per injection cohort; group sizes are summarized in Fig. 1C). Prior to any injections, a random number generator was used to assign one animal to the VEH group, and in four of the injection cohorts, a separate VEH_A group was randomly chosen (Table 1; see following paragraph for a description of the VEH_A animals). At 40 min post-DFP injection, animals that had achieved consecutive seizure behavior scores of ≥3, were randomized using a random number generator into the three remaining treatment groups (DFP, DFP + DZP, DFP + MDZ). When there were sufficient numbers of DFP-injected animals that met the inclusion criteria, a subset of animals were enrolled in the DFP_A group (described in the following paragraph). Animals not enrolled in the present study, including animals

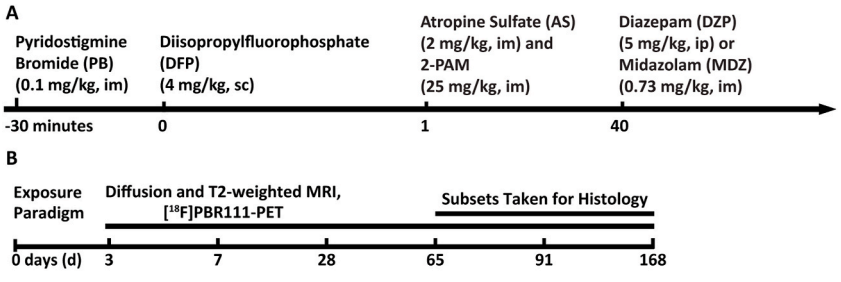

C

Groups	Treament	Scans (n= Designed [Achieved]) / Timepoint (d) 3	7	28	65	91	168
VEH	Saline, PB, AS, 2-PAM, Saline	10 [9]	10 [9]	10 [9]	10 [9]	7 [6]	4 [3]
DFP	DFP, PB, AS, 2-PAM, Saline	10	10 [8]	10	10	7	4
DFP+DZP	DFP, PB, AS, 2-PAM, DZP	10	10	10	10	7	4
DFP+MDZ	DFP, PB, AS, 2-PAM, MDZ	10	10	10	10	7	4
VEH	Saline, PB, AS, 2-PAM, Saline	N/A					4
DFP	DFP, PB, AS, 2-PAM, Saline						4

Fig. 1. Schematic of the study design. (A) Schematic depicting the dosing paradigm used to induce *status epilepticus* while minimizing death. (B) Schematic depicting the experimental timeline for imaging. Animals were imaging longitudinally from 3 to 65 days post-DFP exposure with the exception of two animals in the DFP group that died prior to imaging at the 7 day time point. These animals were replaced with two time-matched DFP intoxicated animals at subsequent time points. Subsets of these animals were imaged at 95 and 168 days. Data in brackets represent the achieved scans at each time after accounting for animal death. (C) Table detailing animal numbers and compounds administered to each experimental group (vehicle control group = VEH).

Table 1
Correlation of Day 3 Imaging Metrics with Day 65 Ventricular Volume (bolded p-values remained significant after FDR correction).

Metric	Region	ρ (95% CI)	p-value
SUV	Hippocampus	0.40 (0.09–0.63)	**0.011**
	Thalamus	0.40 (0.10–0.64)	**0.010**
	Piriform Cortex	0.40 (0.09–0.63)	**0.011**
	Cerebral Cortex (Inner)	0.39 (0.09–0.63)	**0.011**
	Cerebral Cortex (Outer)	0.39 (0.08–0.62)	**0.014**
	Caudate Putamen	0.40 (0.10–0.64)	**0.009**
SUVR	Hippocampus	0.45 (0.15–0.67)	**0.004**
	Thalamus	0.48 (0.20–0.69)	**0.001**
	Piriform Cortex	0.36 (0.05–0.61)	0.021
	Cerebral Cortex (Inner)	0.44 (0.14–0.66)	**0.004**
	Cerebral Cortex (Outer)	0.41 (0.11–0.65)	**0.007**
	Caudate Putamen	0.43 (0.13–0.66)	**0.005**
ADC_{SD}	Hippocampus	0.39 (0.08–0.63)	**0.013**
	Thalamus	0.39 (0.08–0.63)	**0.013**
	Piriform Cortex	0.42 (0.12–0.65)	**0.006**
	Cerebral Cortex (Inner)	0.45 (0.16–0.67)	**0.003**
	Cerebral Cortex (Outer)	0.36 (0.05–0.61)	0.022
	Caudate Putamen	0.24 (−0.08–0.52)	0.134
ADC_{mean}	Hippocampus	−0.03 (−0.34–0.29)	0.860
	Thalamus	−0.41 (−0.64–−0.11)	**0.009**
	Piriform Cortex	−0.27 (−0.54–0.05)	0.092
	Cerebral Cortex (Inner)	−0.29 (−0.55–0.03)	0.071
	Cerebral Cortex (Outer)	−0.13 (−0.43–0.19)	0.424
	Caudate Putamen	−0.16 (−0.45–0.16)	0.325

Abbreviations: SUV, standardized uptake value; SUVR, SUV ratio to cerebellar reference region; ADC_{SD}, standard deviation of the apparent diffusion coefficient; ADC_{mean}, mean of the apparent diffusion coefficient; ρ, Spearman's rank correlation coefficient; C.I., confidence interval.

with low seizure scores, were utilized in other studies (Gonzalez et al., 2020).

2.3. In vivo imaging and analysis

Longitudinal MRI and TSPO PET experiments using the [^{18}F]PBR111 radiotracer (reviewed in Van Camp et al., 2010) were performed at the University of California Davis Center for Molecular and Genomic Imaging at 3, 7, 28, 65, 91, and 168 days post-DFP or vehicle exposure. A subset of the VEH and DFP group animals (VEH_A and DFP_A, respectively) were imaged only at 168 days to evaluate the effect of repeated isoflurane anesthesia on imaging and histological (Supasai et al., 2020) metrics. At the time of imaging, animals were anesthetized with isoflurane (Piramal Healthcare, Bethlehem PA)/O_2 using 2.0–3.0% vol/vol to induce anesthesia and 1.0–2.0% vol/vol to maintain anesthesia. Anesthetized animals were placed in a stereotaxic head holder consisting of ear and bite bars to prevent motion and imaged for up to 1 h for PET and 1.5 h for MRI. Throughout imaging, the animal's body temperature was maintained at 37 °C using warm air or a heat lamp, and anesthesia was adjusted to maintain a respiration rate of 50–70 breaths per min.

After completing the 65-, 91-, and 168-day imaging time points, a subset of animals from each treatment group (DFP, DFP + MDZ, DFP + DZP, VEH) was euthanized for histology (n = 3 after 65 days, n = 3 after 91 days, and n = 4 at 168 days). Animals imaged at the 91-day and 168-day time points additionally underwent *in vivo* CT scanning prior to euthanasia. The histologic assessment and CT data are the topic of a separate publication (Supasai et al., 2020) and, therefore, will not be discussed further here.

2.4. Magnetic resonance imaging (MRI)

MRI scans were performed as previously described (Hobson et al., 2017b) using a Bruker Biospec 70/30 (7T) preclinical MR scanner running Paravision 5.1 (Bruker BioSpin MRI, Ettlingen, Germany), equipped with a 116-mm internal diameter B-GA12S gradient (450 mT/m, 4500 T/m/s), a 72-mm internal diameter linear transmit coil, and a four-channel, rat-brain phased array in cross-coil configuration for signal reception. Multi-slice, T_2-weighted (T2w), fast spin echo (Rapid Acquisition with Repeated Echoes, RARE) axial images were collected as described previously (Hobson et al., 2017b) using the following parameters: repetition time (TR) = 6100 ms; echo time (TE) = 15 ms; RARE factor = 8; averages = 4; field of view (FOV) = 35 × 25 mm^2, with an in-plane data matrix of 280 × 200, resulting in a data set resolution of 0.125 × 0.125 mm^2; 44 slices with a 0.5 mm thickness spanning approximately 7.5 to −13.5 bregma. Diffusion-weighted imaging (DWI) data were collected using a multislice, multishot, 2D gradient echo planar imaging pulse sequence with the following parameters: TR = 5500 ms, TE = 30 ms, FOV = 35 × 25 mm^2 (280 × 200 data matrix), 22 slices with a 0.5 mm thickness centered in the middle of the T2w FOV, 3 diffusion-encoding directions with b = 1600 s/mm^2, 8 segments, 5 averages, and 4 repetitions acquired over 59 min. Total imaging time for each animal was approximately 90 min when accounting for animal positioning within the scanner, shimming, and data acquisition.

Parametric maps of the apparent diffusion coefficient (ADC) were generated using a custom JavaScript macro in FIJI (Schindelin et al., 2012) according to the following equation: $ADC = -(1/b)\ln(S/S0)$ where b is the b-value (Hrabe et al., 2007), S is the signal intensity with diffusion gradients set by the associated b-value, and S0 is the signal intensity without diffusion gradients. Regional ADC histogram metrics (mean (ADC_{mean}) and standard deviation (ADC_{SD}) (Hobson et al., 2017b) were used to quantify the severity of injury.

Brain region volumes of interest (VOIs) and the lateral ventricles were manually segmented by experimenters blinded to treatment group on A0 images (no diffusion weighting; b-value = 0) generated from the DWI scan. Segmentation of the lateral ventricles was performed similarly using T2w images to maximize visual discrepancy of cerebral spinal fluid from surrounding tissue. Segmentation was guided by Paxinos and Watson's *The Rat Brain in Stereotaxic Coordinates* (Paxinos and Watson, 2007), and the axial extent of VOIs, listed as "start/end distance from bregma" in mm, were as follows: caudate putamen 2.0/-2.0; cerebral cortex inner (50% apparent thickness) and outer (50% apparent thickness) 0.0/3.0; hippocampus,-2.0/6.0; piriform cortex, 0.0/-3.5; thalamus (medial and dorsolateral), −1.5/-5.0; lateral ventricles, 0.5/6.0. Image segmentation and extraction of voxel-wise ADC data were performed in the AMIRA 6.0 software (Thermo Fisher Scientific, Waltham, MA), while voxel-wise ADC metrics were calculated in GraphPad Prism v5.01 (GraphPad Software Inc, La Jolla, CA).

2.5. Positron emission tomography (PET)

Automated synthesis of [^{18}F]PBR111 was performed according to previously described methods (Bourdier et al., 2012). PET data were acquired and reconstructed as previously described (Hobson et al., 2019) in one of two preclinical PET systems (Inveon Dedicated PET or microPET Focus 120; both Siemens Medical Solutions, Knoxville, TN, USA). Each animal was imaged on the same scanner at all time points. At the start of data acquisition, a bolus of [^{18}F]PBR111 was delivered by tail-vein injection at an average activity concentration of 38.85 ± 1.85 MBq in 200 μl saline, with the brain located near the center of the field of view of the PET scanner. The scan duration was 1 h, starting 10 s before radiotracer injection. PET data were reconstructed using 2 iterations of the 3-D ordered subset expectation maximization (OSEM3D) method followed by 18 iterations of a maximum a posteriori (MAP) algorithm into two frames (1 × 1200 s, 1 × 2400 s). The reconstruction matrix was 512 × 512 × (95 or 159; scanner dependent) with reconstructed voxel sizes of 0.17 × 0.17 × 0.80 mm^3.

PET images were co-registered to T2w MRI using PMOD v4.0 (PMOD Technologies, Zurich, CHE), the VOIs from MRI were transferred to the PET images and a spherical VOI (3.0 mm diameter) was placed in the center of the cerebellum (approximately −2.75 mm bregma). For each VOI, the standardized uptake values (SUV) and SUV normalized to a

cerebellar region SUV (SUV ratio, SUVR) were calculated over a 40 min frame, starting at 20 min post-injection of the radiotracer. These metrics were previously shown to be highly correlated with histologic and biochemical evidence of neuroinflammation in this model (Hobson et al., 2019; Siso et al., 2017).

2.6. Statistics

Outcome measures included MRI metrics (ADC_{mean}, ADC_{SD}) and PET metrics (SUV, SUVR) across multiple regions of the brain (hippocampus, thalamus, piriform cortex, caudate putamen, inner cerebral cortex, outer cerebral cortex) over time for each animal. In addition, volume of the hippocampus (H) and lateral ventricles (LV) over time for each animal was measured as outcomes. To stabilize the variance to meet assumptions of the analytic approach, all MRI (including volume) and PET metrics were transformed with the natural logarithm. Treatment group (VEH, DFP, DFP + DZP, DFP + MDZ) and days post-exposure (DPE: 3, 7, 28, 65, 91, 185) were also of particular interest. For each outcome, mixed-effects regression models, including animal-specific random effects, were used to assess the overall trajectory over time as well as differences by brain region and treatment group. DPE was treated as a categorical variable. Interactions between region or treatment group and DPE were considered in the models. Akaike information criterion was used for model selection. Specific contrasts testing for differences between DFP and VEH, DFP + DZP and DFP, DFP + MDZ and DFP, and DFP + DZP and DFP + MDZ were constructed and tested using a Wald test. Geometric mean ratios (GMR) are presented for group differences along with 95% confidence interval (CI). If the CI includes 1, there is no significant difference between the groups. Spearman correlations were then computed between volumes at 65 DPE and 3 DPE and regional PET (SUV, SUVR) and MRI diffusion metrics (ADC_{mean}, ADC_{SD}). Within an outcome, Benjamini-Hochberg False Discovery Rate (FDR) (Benjamini and Hochberg, 1995) was used to account for all of the tests conducted across contrasts; FDR correction was also applied to correlations. Comprehensive reporting of geometric mean ratios can be found within Supplemental Materials (Supplemental Tables S1–S3). Unadjusted p-values are presented; results remained significant after FDR, unless otherwise stated. Analyses were conducted using SAS version 9.4.

3. Results

3.1. DFP-induced seizures and mortality

Acute DFP intoxication produced characteristic signs of OP poisoning, including SLUD (salivation, lacrimation, urination, and defecation), tremors, and generalized seizure behavior (seizure behavior score $\geq$3) within 6–8 min of exposure. Data describing the seizure behavior severity and histological analyses of neuropathology of these animals were previously published (Supasai et al., 2020). Across all injection cohorts, 90% (73/81) of animals that received DFP survived at 40 min post-DFP injection. Of DFP animals that did not receive post-exposure intervention with either MDZ or DZP, 89% (47/53) survived to at least 24 h and were enrolled across multiple studies. Among animals enrolled in the present study, survival was as follows: VEH, 90% (9/10); DFP, 83% (10/12); DFP + MDZ, 100% (10/10); and DFP + DZP 100% (10/10). No deaths were observed in the smaller VEH_A (100%; 4/4) and DFP_A, 100% (4/4) cohorts that did not receive longitudinal imaging. The two animals in the DFP group that died on day 7 were excluded from day-7 data analysis, and were replaced with two time-matched, DFP intoxicated rats at the later time points. One animal in the vehicle control (VEH) group died while under anesthesia during the 7-day imaging; all data collected from this animal were excluded from analysis.

Measuring spontaneous recurrent seizures (SRS) arising after the initial SE was not a primary outcome of this study. However, anecdotally, 40% (4/10) of the DFP group displayed transient seizure behavior while awaiting imaging or during handling that was consistent with the behavioral symptoms of SRS, including rearing and falling with limb clonus and loss of righting reflex. By comparison, of the animals in the VEH, DFP + MDZ and DFP + DZP groups, 0% (0/10), 10% (1/10) and 20% (2/10), respectively, exhibited behavioral signs consistent with SRS.

3.2. T_2-weighted (T2w) MRI

In all groups that received DFP, hyperintense brain lesions were apparent in T2w images. These lesions were bilaterally symmetric in incidence and more pronounced in extent and signal intensity during the first week post-exposure than at later time points (Fig. 2). Lesions were observed in the hippocampus, piriform cortex, thalamus, inner and outer cerebral cortex, caudate putamen, septal area, amygdala, and substantia nigra, although incidence and visual extent of hyperintensity varied by animal and time point. In addition to T2w hyperintensity, subsets of scans from animals intoxicated with DFP presented with focal, hypointense (dark) lesions with discrete borders consistent with microhemorrhages in the piriform cortex (VEH, 0/10; DFP, 6/10; DFP + MDZ, 4/10; DFP + DZP, 1/10) and hippocampus (VEH, 0/10; DFP, 3/10; DFP + MDZ, 0/10; DFP + DZP, 0/10). Lesions were approximately 0.5 mm in diameter, generally spherical or ellipsoidal, distinct from large blood vessels and most apparent at 3-, 7-, and 28-d post-exposure (Supplemental Fig. 1). At 28 d, hyperintensity had resolved across regions; however, significant enlargement of the ventricular structures including the lateral and third ventricles and cerebral aqueduct were apparent (Figs. 2–3). Additionally, amorphous hypointense lesions in the thalamus appeared and persisted at 168 d (6 month) post-exposure. These hypointense lesions were generally larger and more irregularly shaped compared to the hypointense lesions in the piriform and hippocampus at earlier time points. These chronic neuropathologies were also apparent in scans of the DFP_A group, which was only imaged at 6-months post-exposure. At no time point were lesions observed in the VEH and VEH_A groups or in the cerebellum of any group.

Quantitative analysis of lateral ventricular volumes revealed that DFP-exposed animals exhibited larger CSF volumes than VEH animals on all days but day 3 (day 7: $p < 0.001$; day 28: $p = 0.001$; day 65: $p < 0.001$; day 91: $p < 0.001$; day 168: $p < 0.001$) (Fig. 3). Treatment with MDZ or DZP significantly reduced the ventricular volumes compared to untreated DFP animals (after FDR correction) on days 65, 91, and 168 for MDZ and on days 7, 65 and 91 for DZP. There were no significant differences between MDZ and DZP-treated animals after FDR correction, and neither of these groups was significantly different from VEH animals (Supplemental Table 1).

Further quantification of hippocampal volumes indicated that mean hippocampal volumes were increased in animals exposed to DFP relative to VEH animals on day 3 ($p < 00.001$), but lower on day 28 ($p = 0.02$), day 65 ($p = 0.02$) and day 91 ($p = 0.02$); only the larger volumes on day 3 were significant after FDR correction (Fig. 3). MDZ-treated animals had reduced hippocampal volumes at day 3 ($p = 0.04$), but larger volumes on days 28 ($p < 0.001$), 65 ($p = 0.047$) and 91 ($p = 0.03$) compared to untreated DFP animals; only the larger volumes on day 28 remained significant after FDR correction. Animals treated with DZP exhibited larger hippocampal volumes, on average, than untreated DFP animals on days 7 ($p = 0.02$), 28 ($p < 0.001$), 65 ($p = 0.002$) and 91 ($p < 0.001$); all but the difference at day 7 remained significant after FDR correction. When comparing the DFP + MDZ and DFP + DZP groups, DFP + DZP animals had larger hippocampal volumes on day 91 ($p = 0.007$). Compared to the VEH group, the DFP + DZP group had larger hippocampi on day 3 ($p < 0.001$) and 91 ($p < 0.001$), while there were no significant differences between the DFP + MDZ and VEH groups.

3.3. Diffusion-weighted MRI

Diffusion-weighted MRI displayed lesions in the same brain regions

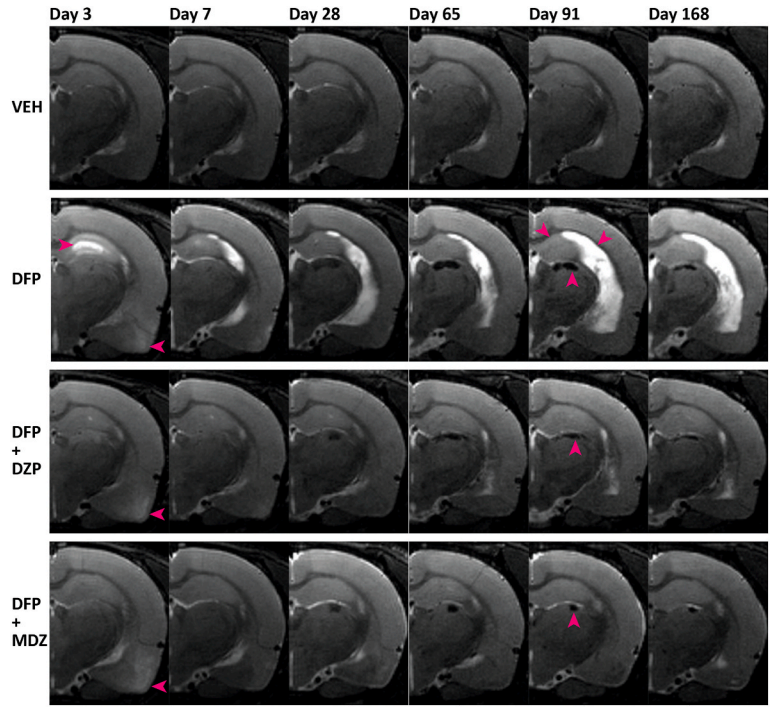

Fig. 2. Acute DFP intoxication produces lesions and signs of brain atrophy evident in T2w images that are attenuated by intervention with DZP or MDZ. Rows are representative axial (−3.5 mm bregma) T2w images of the left hemisphere of a single animal from each experimental group. A vehicle control animal (row 1) shows homogeneous image intensity in brain parenchyma that is consistent across follow-up scans. By comparison, the DFP animal (row 2) displays hyperintense lesions in the hippocampus (arrowhead right) and piriform cortex (arrowhead left). At later time points, this animal is characterized by progressive hippocampal atrophy (arrowhead down right), profound ventricular enlargement (arrowhead down left), and hypointense lesions within the thalamus (arrowhead up). Intervention with DZP (row 3) or MDZ (row 4) appeared to prevent hippocampal hyperintensity, but not hyperintensity within the piriform cortex nor hypointensity within the thalamus. Note: not all lesions are marked by arrowheads in the array of images.

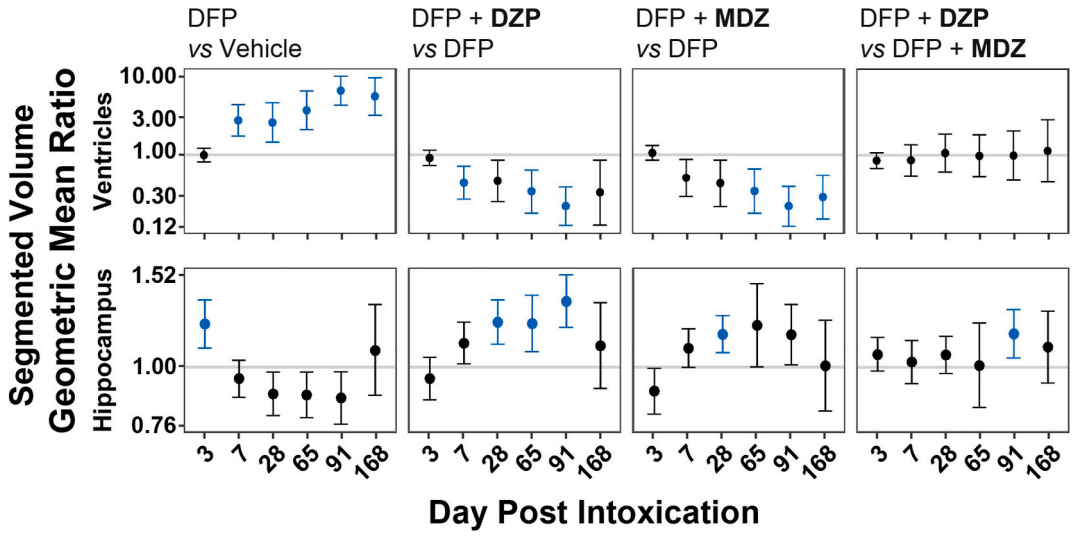

Fig. 3. Quantification of lateral ventricular and hippocampal volumes following acute DFP intoxication demonstrate ongoing brain atrophy that is reduced by DZP and MDZ intervention. Geometric mean ratios (GMR) depict changes in regional volumes over time relative to a comparator group. Columns represent specific comparisons between experimental groups; rows represent distinct brain regions compared at each imaging time point. Given the rodent skull maintains approximately a fixed volume in adulthood, enlargement of the lateral ventricles represents a recession of brain tissue as CSF increases to fill the space available. Data are presented as the GMR (dot) with 95% confidence interval (vertical bars) from days 3 through 168 post-exposure); the horizontal line corresponds to a GMR of 1.0 (Days 3–65, n = 8–10 animals per group; days 91 and 165; n = 3–7 animals per group). Confidence intervals that do not include 1.00, and survived correction for multiple comparisons (FDR), are colored blue and indicate a significant difference between the two groups being compared at $p < 0.05$.

as T2w images. Compared to the observed T2w hyperintensity, lesions on diffusion-weighted images were heterogeneous in intensity except for thalamic lesions at late time points, which appeared hypointense (Figs. 2 and 4). Analysis of mean regional ADC (ADC_{mean}) revealed treatment differences that varied across days and regions (Supplemental Fig. 2). ADC_{mean} values were lower on average in DFP animals compared to VEH controls in all regions ($p < 0.001$) except the piriform cortex on day 3. At day 7, no significant differences were identified in mean ADC between

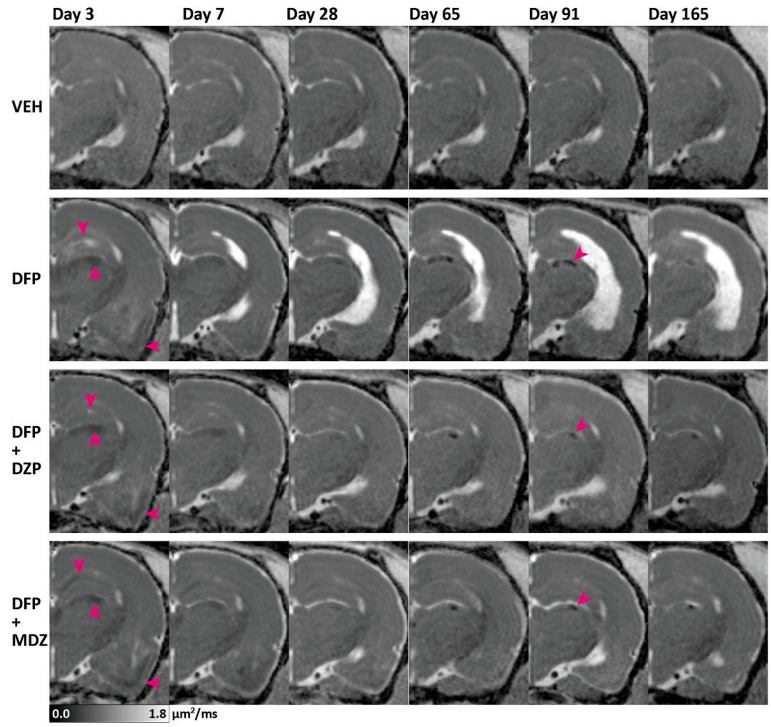

Fig. 4. Acute DFP intoxication produces aberrant tissue diffusion characteristics that are brain region-specific and not resolved by intervention with DZP or MDZ. Rows are representative axial (−3.5 mm bregma) parametric maps of the ADC calculated from diffusion-weighted MRI of a single animal from each experimental group. Comparison of a VEH control animal (row 1, VEH) to animals that received DFP, with or without benzodiazepine intervention (rows 2, 3, and 4), reveals persistent lesions in the hippocampus (arrowhead down), thalamus (arrowhead up), and piriform cortex (arrowhead left) characterized by areas of increased ADC heterogeneity. Diffusion-weighted MRI also reveals hippocampal atrophy and ventricular enlargement following DFP intoxication with saline intervention. Note: not all lesions are marked by arrowheads in the array of images.

DFP animals and VEH, although visual inspection of ADC maps indicated localized, intra-regional areas of elevated or restricted ADC corresponding spatially to hyperintensity on T2w images. By day 28, ADC_{mean} values were higher in DFP animals in the piriform cortex ($p = 0.002$), which remained higher through day 91 compared to vehicle controls ($p < 0.002$). On day 91, higher values were also observed in caudate putamen ($p = 0.002$). There were no significant regional differences in mean ADC between the DFP, DFP + MDZ or DFP + DZP groups that survived FDR correction. Similarly, no significant differences were detected at the final (6-month) time point between DFP or VEH groups compared to their peers that were imaged only at the 6-month time point (DFP_A and VEH_A) though it is worth noting animal group sizes, and thus statistical power, were reduced ($n = 3–7$) at this final time point.

Analysis of tissue heterogeneity using regional ADC standard deviation (ADC_{SD}) indicated that this metric was markedly higher in DFP than VEH animals in all regions, except the caudate putamen and inner cerebral cortex, on day 3 ($p < 0.008$), day 7 ($p < 0.006$), day 28 ($p < 0.001$), day 65 ($p < 0.001$), day 91 ($p < 0.001$), and day 168 ($p < 0.001$). In the caudate putamen, the ADC_{SD} did not differ between DFP and VEH on any day post-exposure; in the inner cerebral cortex a significant difference between these groups was detected only at day 7 ($p = 0.0058$) (Fig. 5). At the 6-month time point, remaining animals in the DFP group ($n = 7$) had higher ADC_{SD} in the hippocampus ($p < 0.001$) compared to their DFP_A group ($n = 4$) peers that were imaged only at the 6-month time point. Conversely, the remaining VEH group ($n = 3$) had lower ADC_{SD} than the VEH_A group ($n = 4$) in the outer cerebral cortex ($p < 0.001$), hippocampus ($p = 0.002$) and thalamus ($p = 0.009$).

When compared to the DFP group, the DFP + MDZ group had lower ADC_{SD} in the hippocampus than their counterparts in the DFP group at all time points (days 3 ($p < 0.01$), 7 ($p < 0.01$), 28 ($p < 0.01$), 65 ($p < 0.01$), day 91 ($p < 0.002$), and day 168 ($p = 0.01$)), the inner cerebral cortex at days 3 ($p = 0.01$), 7 ($p < 0.001$), 28 ($p < 0.01$), and 91 ($p = 0.002$), the outer cerebral cortex on days 7 ($p < 0.001$), 28 ($p < 0.01$), 65 ($p < 0.02$), and 91 ($p < 0.002$), and the other regions on day 7 ($p < 0.01$). Animals in the DFP + DZP group had lower ADC_{SD} than the DFP group in all regions at all time points (days 3 ($p < 0.01$), 7 ($p < 0.002$), 28 ($p < 0.002$), 65 ($p < 0.002$), 91 ($p < 0.002$), 168 ($p < 0.002$)) with the following exceptions: the thalamus and caudate putamen on days 3, 28, 65, 91, 168, and all other regions but the hippocampus at day 168. Results at day 168 may have been influenced by limited samples sizes (Table 1). There were no differences between DFP + MDZ and DFP + DZP in any region at any time point.

3.4. Neuroinflammation detected by [^{18}F]PBR111 TSPO PET

Visual inspection of [^{18}F]PBR111 PET imaging data at 3 days post DFP intoxication revealed marked increases in radiotracer uptake in cortical and subcortical areas when compared to vehicle controls (Fig. 6). Patterns of radiotracer uptake were highly consistent across vehicle controls, but varied slightly from animal-to-animal in groups that underwent DFP intoxication. Following DFP intoxication, lesions presenting with increased uptake of [^{18}F]PBR111 were most reliably observed in the piriform cortex, amygdala, and thalamus; however, lesions were also observed in the hippocampus, motor and cerebral cortices, and rarely the caudate putamen. Intervention with MDZ or DZP reduced the visual appearance of [^{18}F]PBR111 uptake relative to DFP alone, but lesions frequently remained in the piriform cortex and amygdala. Little to no uptake of [^{18}F]PBR111 was observed in the cerebellum of any animal at any timepoint consistent with previous imaging (Hobson et al., 2019) and histological studies (Siso et al., 2017).

Acute DFP intoxication significantly increased uptake of the [^{18}F]PBR111 tracer as assessed by SUV (Supplemental Fig. 3), and SUVR (Fig. 7) in all assessed regions at all time points out to 91 days post-

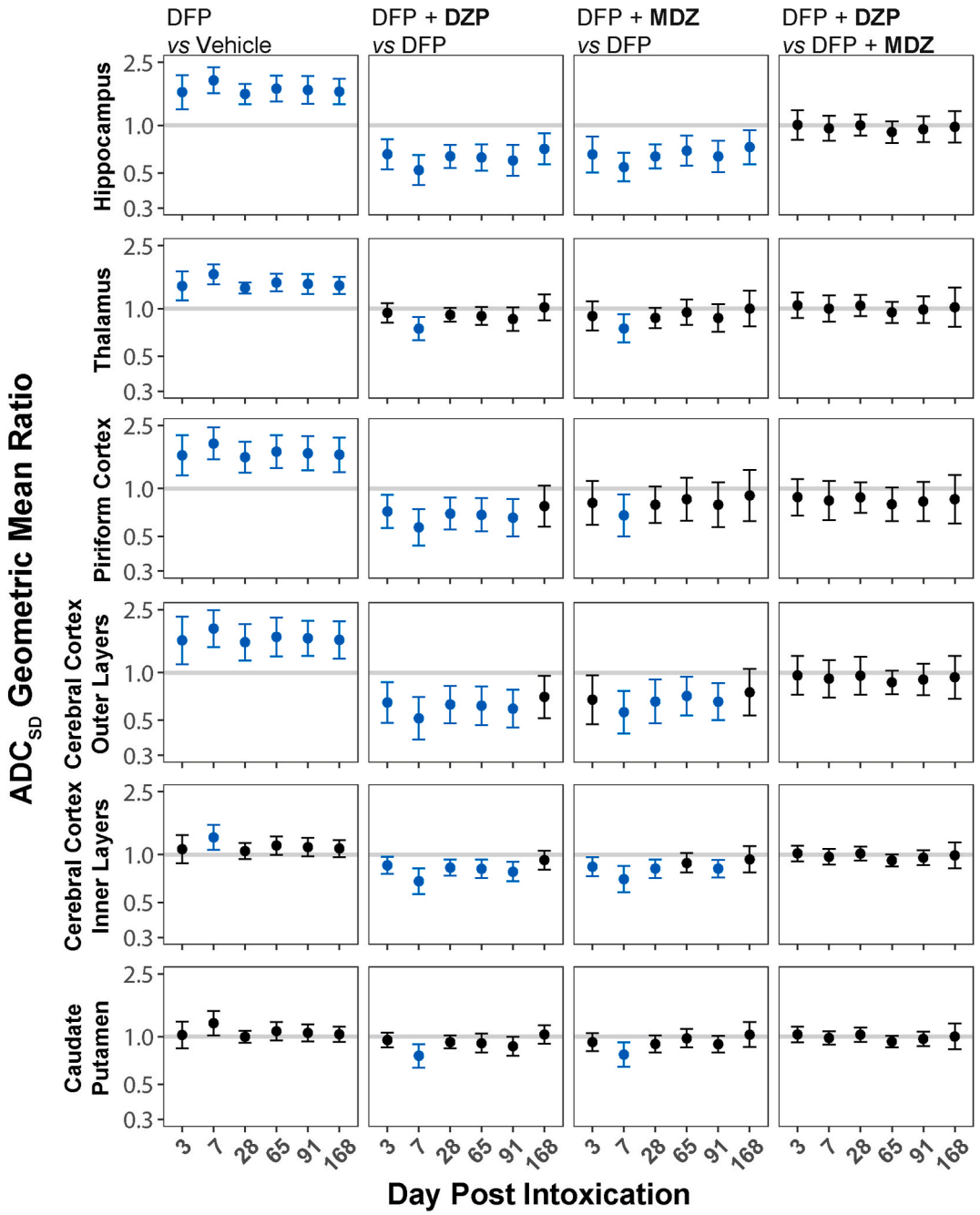

Fig. 5. Spatiotemporal quantification of ADC heterogeneity demonstrates persistent region-specific damage following acute DFP intoxication, with or without benzodiazepine intervention. Columns represent specific experimental groups; rows represent distinct brain regions at each imaging time point. Data are presented as the geometric mean ratio with 95% confidence interval (Day 3–65, n = 8–10 animals per group; days 91 and 165: n = 3–7 animals per group). Confidence intervals that do not include 1.00 and survived correction for multiple comparisons are colored blue and indicate a significant difference between groups at $p < 0.05$.

exposure ($p < 0.001$ and $p < 0.01$, respectively). Although sample sizes were lower at the final 168-day time point (Table 1), SUVR showed a significant difference in the hippocampus and inner cerebral cortex ($p < 0.01$). There were no significant differences in SUV or SUVR in any region between DFP and DFP_A or between VEH and VEH_A groups.

When compared to the DFP group, the DFP + MDZ group had reduced SUV compared to DFP in the cerebral cortical regions on day 3 ($p < 0.006$) and day 7 (outer only, $p = 0.01$). On days 28, 65 and 91, SUV was significantly reduced in all regions ($p < 0.002$, $p < 0.001$, and $p < 0.005$, respectively), except the piriform cortex at all time points, the caudate putamen (days 28 and 91), and thalamus on day 91. There were no differences detected in animals remaining on day 168. In terms of SUVR, compared to the DFP group, DFP + MDZ animals had reduced [18F]PBR111 uptake in the hippocampus (day 3, $p < 0.01$; day 28, $p < 0.02$; day 168 $p < 0.01$), outer cerebral cortex (all except day 91, $p < 0.01$), and inner cerebral cortex (day 3, $p < 0.01$; day 28, $p < 0.02$; day 168, $p < 0.01$).

Post-exposure intervention with DZP reduced SUV in the outer cerebral cortex on days 3 ($p = 0.01$), 28 ($p < 0.001$), and 65 ($p < 0.001$), as well as in the hippocampus and inner cerebral cortex at day 28 ($p = 0.008$). Similarly, the DFP + DZP group had significantly reduced SUVR relative to DFP in the outer cerebral cortex at day 7 ($p = 0.008$). There

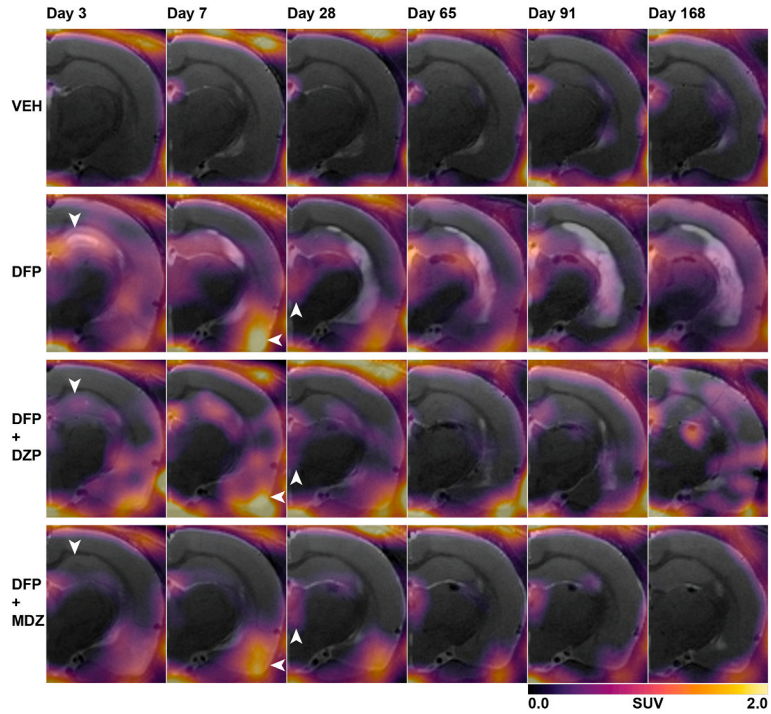

Fig. 6. Persistent neuroinflammation in the thalamus and piriform cortex resulting from acute DFP intoxication is unaffected by diazepam or midazolam intervention. Longitudinal PET SUV maps of a single animal from each experimental group. Data are overlaid on T2w images from the same animal (Fig. 2). The [^{18}F]PBR111 uptake observed in the vehicle animal is largely due to non-specific binding along major blood vessels and outside the brain. By comparison, the DFP animal displays significant radiotracer uptake in the hippocampus (arrowhead down), thalamus (arrowhead up), and piriform cortex (arrowhead left) that persists for the duration of the study. Diazepam or midazolam intervention attenuates, but does not prevent, apparent radiotracer uptake in the thalamus and piriform cortex. Midazolam intervention appears to reduce radiotracer uptake in the hippocampus of this particular animal. In all scans there is minor signal penetration from outside the brain along the skull and jaw bones due to [^{18}F] binding in bone following defluorination of the radiotracer. Note: not all inflammatory lesions are marked by arrowheads in the array of images.

were no other differences between DFP + DZP and DFP animals.

No differences were observed between DFP + MDZ and DFP + DZP treated animals in terms of SUV or SUVR at any time point in any region, except that DFP + MDZ animals had a lower SUVR than DFP + DZP animals in the inner cerebral cortex on day 3 ($p = 0.007$).

3.5. Early MRI and PET metrics are positively correlated with long-term brain atrophy

Correlation between day 3 TSPO PET and diffusion MRI metrics with day 65 ventricular volumes across all groups yielded significant, although modest, positive associations (Table 1). Higher levels of neuroinflammation as assessed by TSPO PET SUV and SUVR in all regions at day 3 were associated with larger ventricular volumes at day 65, although the correlation with SUVR in the piriform cortex did not remain significant after FDR correction. Higher mean ADC at day 3, suggestive of reduced cytotoxic edema (reviewed in Obenaus and Jacobs, 2007), in the thalamus was associated with smaller ventricular volumes at day 65 ($\rho = -0.41$; 95% CI $= -0.64, -0.11$; $p = 00.008$), and higher ADC_{SD} in all regions at day 3, except for the caudate putamen, was associated with higher ventricular volumes at day 65; however, the correlation in the outer cerebral cortex did not remain significant after FDR. Significant correlation between imaging metrics and hippocampal volume was limited to ADC_{SD} in the inner cerebral cortex, with higher ADC_{SD} at day 3 associated with lower hippocampal volumes at day 65 ($\rho = -0.59$; 95% CI $= -0.76, -0.33$; $p < 00.001$).

3.6. Imaging metrics are highly correlated with severity of seizure behavior

Average severity of seizure behavior during the first 4 h following DFP intoxication was highly correlated with SUV and SUVR when pooling across regions, time points, or both region and time point (Supplemental Table 4). ADC_{SD} was significantly correlated with severity of seizure behavior, except in the caudate putamen and inner cerebral region ($p = 0.49$ and 0.10, respectively).

Higher seizure scores were associated with lower hippocampal volumes ($\rho = -0.34$; 95% CI $= -0.59, -0.3$; $p = 0.03$) and larger ventricular volumes ($\rho = 0.57$; 95% CI $= 0.31, 0.75$; $p < 0.001$) at day 65; however, only the correlation with ventricular volume remained significant after FDR correction.

4. Discussion

The present study employed TSPO PET and T2w and diffusion MRI to longitudinally interrogate neuropathology and neuroinflammation following acute DFP intoxication up to approximately 6 months (168 days) post-exposure using a panel of quantitative imaging metrics. To date, the resulting data and analysis represent the most comprehensive *in vivo* imaging-based assessment of acute OP intoxication in any preclinical model (Bar-Klein et al. 2016, 2017; Bhagat et al. 2001, 2005; Carpentier et al., 2008; Gullapalli et al., 2010; Hobson et al. 2017a, 2017b, 2019; Reddy et al., 2020; Rosman et al., 2012; Shrot et al., 2012; Swissa et al., 2020; Testylier et al., 2007), and one of the largest *in vivo* imaging-based assessments in a preclinical seizure model (Blumenfeld, 2007; Dietrich et al., 2016; Kharatishvili et al., 2014; Reddy et al., 2019; Roch et al., 2002; Salo et al., 2017; Tokumitsu et al., 1997; van Vliet et al., 2016). The results of this study demonstrate that a single exposure to DFP at a level that triggers acute SE results in profound and progressive brain atrophy and multiple distinct lesion types apparent on T2w and diffusion MR images that vary by brain region and time post-exposure. These neuropathological lesions, which persisted up to 6

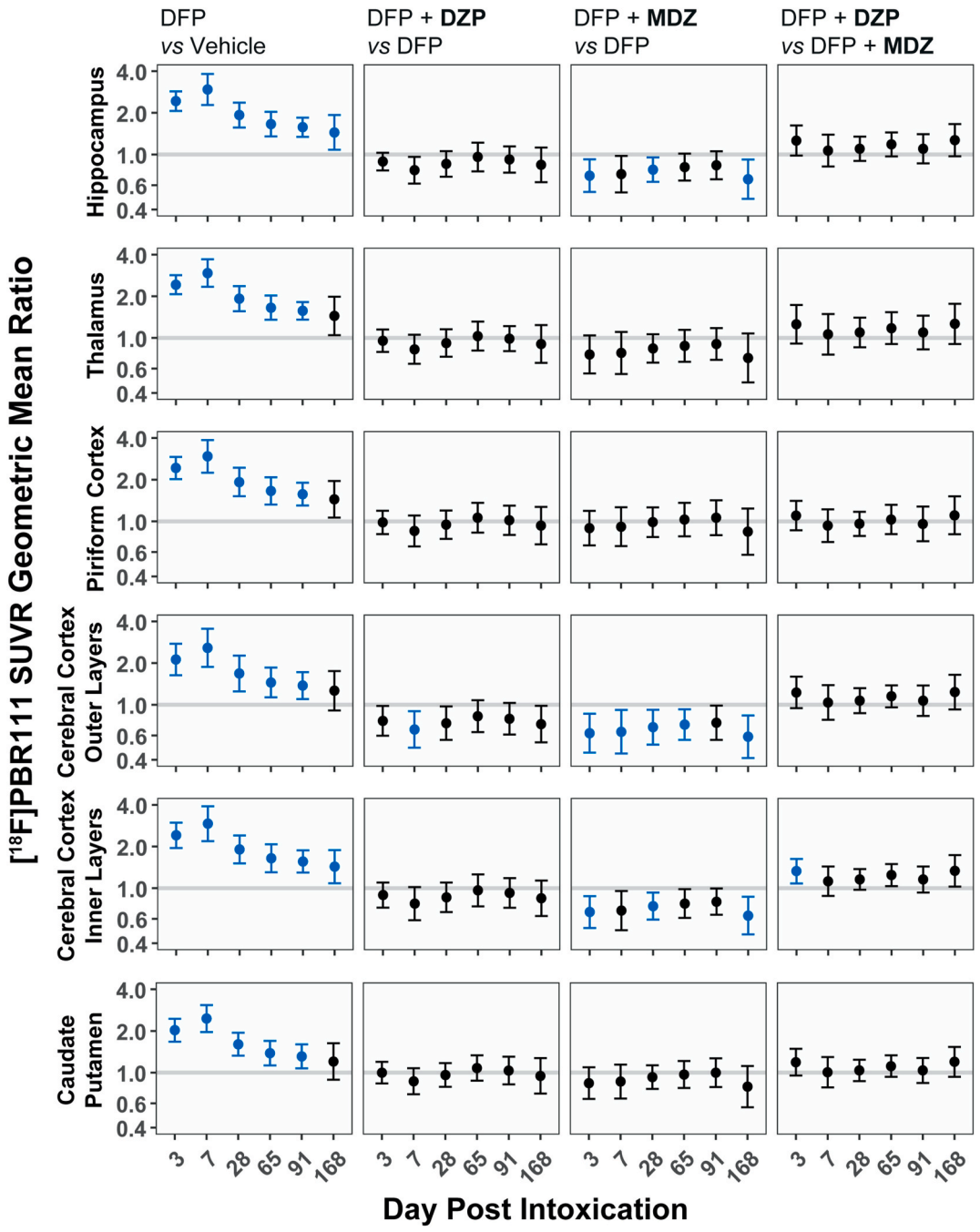

Fig. 7. Chronic neuroinflammation following acute DFP intoxication persists in multiple regions even with midazolam or diazepam intervention. Regional [^{18}F]PBR111 uptake data quantified by standard uptake value (SUV) analysis normalized to the SUV of a cerebellar reference region (SUVR). Columns represent specific experimental groups; rows represent distinct brain regions at each imaging time point. Data are presented as the geometric mean ratio (dot) with 95% confidence interval (vertical bars); the horizontal line corresponds to a GMR of 1.0 (Days 3–65, n = 8–10 animals per group; days 91 and 165; n = 3–7 animals per group). Confidence intervals that do not include 1.00, and survived correction for multiple comparisons (FDR), are colored blue and indicate a significant difference between the two groups being compared at $p < 0.05$.

months post-exposure, coincided with persistent neuroinflammation. Early indices of neuropathology and neuroinflammation were significantly associated with long-term brain atrophy. Critically, the efficacy of benzodiazepine therapy in attenuating or mitigating these processes varied markedly by brain region, with several areas experiencing severe injury despite intervention with either MDZ or DZP. Finally, longitudinal imaging had subtle, but significant, effects on the severity of injury compared to a single imaging session.

4.1. *DFP-induced ventriculomegaly as evidence of atrophy*

We observed pronounced ventriculomegaly in the weeks following acute DFP intoxication consistent with the magnitude and temporal progression of this neuropathological outcome previously reported following acute OP intoxication in humans (reviewed in Figueiredo et al., 2018) and rodent models (Gullapalli et al., 2010; Hobson et al., 2017b; Reddy et al., 2020; Rosman et al., 2012). Despite its recognition as a long-term consequence of OP poisoning, the status of ventricular enlargement beyond the first month post-OP intoxication has remained

poorly characterized. Our data indicate ventriculomegaly is readily detectable 7 d post-DFP and increases in severity until stabilizing between 3- and 6-months post-DFP. Additionally, we observed a downward trend in hippocampal volume over the same period; however, whether reduced hippocampal volume is a cause or effect of the ventriculomegaly remains unclear. Ventriculomegaly commonly results from dysfunction in CSF dynamics (i.e., flow or fluid production), known as communicating or non-communicating hydrocephalus (Leinonen et al., 2017), or alternatively, hydrocephalus *ex vacuo*, where CSF expands to occupy intracranial space vacated by receding brain tissue. In all cases, CSF and tissue volumes are inversely related. While we were unable to assess CSF flow or pressure, a canonical histopathological finding in rodent models of OP poisoning is widespread neuronal necrosis during the first week post-intoxication (Collombet, 2011) as observed in mice (Baille et al., 2005), rats (Guignet et al., 2020; Siso et al., 2017) and guinea pigs (McDonough and Shih, 1997). This frank cellular loss would precede, and progress concurrently (de Araujo Furtado et al., 2010; Siso et al., 2017) with *in vivo* imaging detection of ventricular enlargement at later time points, suggesting that ventricular enlargement in the rat model of acute DFP intoxication reflects hydrocephalus *ex vacuo*. In addition, we did not observe any compression or compartmentalization of CSF structures in the cerebellum, cerebral aqueduct, or ventricular structures that would suggest disruption of CSF flow characteristic of non-communicating hydrocephalus (reviewed in Langner et al., 2017). Nonetheless, animals from the present study had extensive ongoing neurodegeneration in the hippocampus, thalamus, amygdala, and cerebral and piriform cortices at 3- and 6-months post-intoxication as assessed by FluoroJade-C staining (Supasai et al., 2020). Thus, our data show strong evidence of ventriculomegaly as a marker of atrophy; however, whether CSF dynamics, such as increased ventricular pressure, contribute to persistent OP-induced neuropathology requires further study.

4.2. Diffusion MRI suggest heterogeneous tissue reponses to DFP

Alterations in tissue diffusion characteristics, more commonly reported as reductions in mean ADC, have been reported in clinical (Hubers et al., 2018; Rennebaum et al., 2016) and preclinical (reviewed in Bertoglio et al., 2017; Grohn and Pitkanen, 2007) studies of SE. We observed similar patterns of reduced mean ADC at 3 d post-DFP that largely resolved by 7 d post-exposure, which is in line with previous studies of preclinical OP nerve agent intoxication (Bhagat et al., 2005; Testylier et al., 2007). The similarity in regional distribution and temporal progression of restricted diffusion in preclinical models of acute OP intoxication and SE induced by chemicals other than OPs suggest these early diffusion changes are a consequence of SE. This transient reduction in mean ADC has been extensively documented in animal models of ischemic brain injury (Kuroiwa et al., 2007) in which it has been characterized histologically and biochemically as cytotoxic edema resulting from mass cellular depolarization and swelling prior to necrosis (reviewed in Hartings et al., 2017), although the exact subcellular mechanisms linking restricted diffusion to the observed necrosis remain elusive (reviewed in Ackerman and Neil, 2010).

In contrast to the transient changes in mean ADC, one of the more striking results from the present study was the persistent and robust increase in tissue diffusion heterogeneity (ADC_{SD}) observed within the hippocampus, thalamus, piriform cortex, and cerebral cortex of DFP-intoxicated animals. This increase in ADC_{SD} confirms and extends previous observations in the rat DFP model in which this phenomenon was highly correlated with neuronal necrosis and gliosis during the first month post-intoxication (Hobson et al., 2017b). Furthermore, the persistence of elevated ADC_{SD} at several months after DFP intoxication parallels histological evidence of neurodegeneration, astrogliosis, microgliosis, and calcification in these same animals at 3 and 6 months (Supasai et al., 2020), supporting ADC_{SD} as a sensitive measure of underlying pathology. One explanation for the observed discrepancy between mean- and heterogeneity-based ADC metrics may be local variation in lesion progression within brain regions that is captured by measures of heterogeneity but lost during averaging across a VOI. This is supported by histological assessment identifying persistent, highly localized neuropathology in these animals (Supasai et al., 2020), with similar findings reported in mice (Baille et al., 2005; Collombet, 2011) and rats (Reddy et al., 2020) acutely intoxicated with soman.

4.3. Neuroinflammation isa complex therapeutic target

TSPO PET revealed pronounced increases in [^{18}F]PBR111 uptake that persisted for 3 months in all assessed brain regions and remained elevated at 6 months post-exposure in the hippocampus and cerebral cortex. These results were confirmed by histological staining for IBA1, CD68, GFAP, and S100β in the same animals (Supasai et al., 2020), and collectively demonstrate progressive ongoing neuroinflammation consistent with our previous results using the [^{18}F]PBR111 radiotracer (Hobson et al., 2019). Intriguingly, neuroinflammation appeared most severe preceding and concurrent with the development of ventriculomegaly and a downward trend in hippocampal volume. These observations support the long-standing hypothesis that neuroinflammation contributes mechanistically to the progressive neurodegeneration and necrosis following acute OP intoxication (reviewed in Banks and Lein, 2012; Cowan et al., 2003, Zimmer et al., 1997). Multiple approaches are being evaluated to alter post-intoxication prognosis using anti-inflammatory therapies (reviewed in Andrew and Lein, 2021). These attempts have largely focused on intense suppression of inflammation during the first month post-OP intoxication and have met with mixed success (reviewed in Andrew and Lein, 2021; Rojas et al., 2015). The persistence of neuroinflammation and progressive ventriculomegaly suggests therapeutic intervention with immunomodulators may be more effective if administered at delayed time points, e.g., at one-month post-intoxication or later. While TSPO PET has become a preclinical standard for imaging activated glia (Van Camp et al., 2021), it cannot distinguish between the beneficial versus deleterious cellular phenotypes associated with glial activation (reviewed in Andrew and Lein, 2021). In the present study, all brain regions experienced reduced mean ADC consistent with local necrosis and simultaneously displayed marked neuroinflammation as detected by TSPO PET. At later time points, neuroinflammation persisted in brain regions displaying tissue diffusion characteristics consistent with vehicle controls such as the caudate putamen and inner layers of the cerebral cortex. This discrepancy between MRI-based readouts of neuropathology and PET-based assessment of neuroinflammation, notably using identical VOI segmentations, suggests the role of neuroinflammation may be highly region-specific and time-dependent as has been suggested in other models of preclinical epilepsy (reviewed in Vezzani et al., 2019) and stroke (reviewed in Stuckey et al., 2021).

4.4. Early imaging is not wholly predictive of long-term outcomes

While we observed significant correlations between MRI- and PET-based metrics of early neuropathology and neuroinflammation and long-term brain atrophy, the strength of these associations was modest rather than strongly predictive (Schober et al., 2018). Nonetheless, the significant positive correlation between ADC_{SD} and [^{18}F]PBR111 SUVR at 3 d post-intoxication and generalized brain atrophy at 2 months post-exposures as assessed by ventricular volume suggests the cellular and molecular mechanisms mediating the initial changes in imaging metrics, particularly inflammation, contribute to long-term irreversible loss of brain parenchyma. A similar study in rats comparing *in vivo* MRI metrics of edema during the first week following acute soman intoxication with long-term behavioral assessments observed correlations of similar magnitudes (Shrot et al., 2015). When compared to the strong correlations between temporally matched assessments of histology versus non-invasive MRI (Hobson et al., 2017b; Reddy et al., 2020) and

PET (Hobson et al., 2019), the weaker correlations between early and late readouts of OP-induced brain injury may be due to the onset of secondary morbidity such as spontaneous recurrent seizures (SRS) or epilepsy, which vary significantly between individual animals (de Araujo Furtado et al., 2010; Guignet et al., 2020). While the present study did not explicitly monitor the development of SRS, behavioral signs consistent with SRS were anecdotally observed in a subset of DFP-intoxicated animals. SRS has been shown to exacerbate neuropathology following acute OP intoxication (de Araujo Furtado et al., 2010; Guignet et al., 2020); however, the mechanisms determining whether acute OP intoxication results in SRS remain unclear.

4.5. Diffusion and T2w MRI suggest blood brain barrier dysfunction

The hyperintensity we observed on T2w images was concurrent with aberrant tissue diffusion on parametric maps of ADC, suggesting profound edema containing both vasogenic and cytotoxic components (reviewed in Budde and Skinner, 2018; Dreier et al., 2018). When combined with the evidence of microbleeds in the piriform cortex and hippocampus, these observations suggest dysfunction in the neurovascular unit (NVU), such as blood brain barrier (BBB) breakdown or frank compromise of vessel integrity (reviewed in Michinaga and Koyama, 2015). Exposure to OP pesticides at levels that did not produce acute cholinergic crisis in juvenile rats has been shown to impair the BBB (Gupta et al., 1999; Song et al., 2004), and acute intoxication with OPs has been reported to cause leakage of albumin into brain parenchyma up to 48 h post exposure in rats (Bernardino et al., 2023a). Extravasation of circulating immune cells and/or plasma proteins into brain parenchyma may contribute to the persistent inflammation we observed by TSPO PET imaging (Bernardino et al., 2023a). Assessment of hippocampal volumes at 3 d post-DFP identified an increase in hippocampal volume consistent with swelling following NVU breakdown. This would suggest that therapeutic strategies to decrease edema in the brain following acute OP intoxication may be neuroprotective. While it has been previously reported that administration of hyperosmolar therapies to attenuate vasogenic edema were ineffective in a mouse model of soman poisoning (Carpentier et al., 2008), the intervention was limited to a single dose at 5 h post-soman intoxication. NVU dysfunction has been detected at one week (Bernardino et al., 2023a) and one month (Bar-Klein et al., 2017) post OP intoxication; however the underlying mechanisms behind these effects and their time course remain largely limited to the first few days post OP intoxication (Abdel-Rahman et al., 2002; Bernardino et al. 2023a, 2023b; Rojas et al., 2022). Additional studies are required to characterize the integrity of the NVU and its components, particularly pericytes, following acute OP intoxication. Intriguingly, in this study, we observed that dysfunction in tissue diffusion at 3 d post-DFP was highly correlated with the severity of brain atrophy at 2 months. Collectively, these early and chronic pathologies in CSF volume, tissue fluid volume and diffusion, and vascular compromise implicate blood brain barrier dysfunction as a potential mechanism contributing to acute and chronic neuropathology and inflammation observed following acute intoxication with DFP and other potent cholinesterase inhibiting OPs.

4.6. Impact of longitudinal imaging

While minimal, we observed statistically significant differences between animals receiving 12 imaging sessions (6 MRI and 6 PET) over 6 months post-DFP *versus* those receiving a single MRI at 6 months post-DFP. Specifically, DFP animals that received longitudinal imaging had higher ADC_{SD} in their hippocampi than similarly treated animals that were imaged only once (DFP_A group), while longitudinally imaged VEH animals had lower ADC_{SD} in multiple brain regions relative to VEH animals that were imaged once (VEH_A group). The apparent increase in the variance of diffusion rates within the hippocampus may suggest that repeated handling influenced tissue remodeling, perhaps via effects on neuroplasticity (reviewed in Jones et al., 2003) or on moss fiber sprouting (Blair et al., 2024). Differences detected by diffusion MRI were not observed by TSPO PET suggesting that either the MRI effects are not mediated by differential effects of handling or repeated exposure to anesthesia on gliosis or that the effects on gliosis are too subtle to meaningfully impact PET images, which have lower spatial resolution than MR images. Another consideration is that isoflurane, which was used to anesthetize animals during imaging, has well documented neuroprotective effects in preclinical models of SE (Altay et al., 2014); however, our observations would suggest a subtle increase in hippocampal injury in DFP animals with repeated imaging sessions. This phenomenon may be due to increased handling and transport of animals used for longitudinal imaging, as these events may trigger spontaneous recurrent seizures (Guignet et al., 2020), potentially exacerbating injury. Animals in the longitudinally imaged DFP group displayed seizure behavior proximal to imaging that was consistent with SRS; however, we did not conclusively identify SRS nor quantify its frequency in the present study. Finally, there was a trend, though not significant, towards lower average severity of acute SE in the DFP_A group despite randomization. Given the strong association between seizure severity and brain injury, this difference may account for the subtle increase in neuropathology in DFP group relative to the DFP_A group. Future purpose-built studies are warranted to evaluate how longitudinal imaging impacts brain injury where handling or anesthesia may impact progression of damage or recovery.

4.7. Neuroprotective limitations of delayed DZP and MDZ

The standard of care for treating acute OP intoxication includes management of seizure activity with benzodiazepines (FDA, 2018; Krutak-Krol and Domino, 1985; McDonough and Shih, 1997; reviewed in Newmark, 2019). In 2018, the FDA identified MDZ as superior to DZP for treating SE, in part because of preclinical data demonstrating attenuated neuropathology (FDA, 2018; Krutak-Krol and Domino, 1985) and clinical trials highlighting its ease of application relative to DZP (McMullan et al., 2010; Silbergleit et al., 2011). However, recent evaluation of these agents in rodent models of acute OP intoxication indicate variable performance between the two therapeutics (Kuruba et al., 2018; Supasai et al., 2020; Wu et al., 2018b), particularly when administration is delayed to emulate clinical timelines following suicides, accidental exposures and civilian mass casualties (Arca et al., 2020; Heemskerk et al., 2022; Hill et al., 2017; Kapur et al., 2019; Kim et al., 2018; Kirschenbaum et al., 2005; Pfenninger et al., 2020; Power et al., 2016; Vardell, 2012). In the present study, intervention with MDZ or DZP administered 40 min after DFP attenuated regional SUV metrics of neuroinflammation, atrophy, and aberrant ADC values following DFP intoxication; however, these effects were highly region- and time-dependent. Critically, neither MDZ nor DZP significantly attenuated the reductions in mean ADC observed across brain regions during the first week following DFP. Reductions in mean ADC have been correlated with acute neuronal necrosis across preclinical models of stroke (Li et al., 2000), epilepsy (Yogarajah and Duncan, 2008) and acute OP intoxication (Bhagat et al., 2001; Hobson et al., 2017b). In the present study, parametric maps of mean ADC revealed that areas of restricted diffusion corresponded to neuronal cell layers within hippocampus, amygdala, piriform cortex, and dorsal thalamus, all areas with well documented neuronal necrosis following acute OP intoxication (Collombet, 2011; Hobson et al., 2017b; Siso et al., 2017). Collectively, these lines of evidence suggest neither benzodiazepine, when administered at delayed times after onset of OP-induced SE, adequately protect the brain from significant neuronal cell death.

While both MDZ and DZP were effective in reducing DFP-mediated increases in ADC_{SD} in the hippocampus, neither therapy was consistently effective across the other brain areas. Of note, ADC_{SD} indicated the piriform and thalamus continued to exhibit severe lesions following DFP intoxication despite MDZ or DZP intervention, and TSPO PET similarly demonstrated neither therapy was able to significantly reduce

neuroinflammation in those brain regions. These findings are consistent with histological evidence of neurodegeneration and microglial activation in these regions at 6 months post-intoxication that was not significantly different than levels observed in DFP animals that did not receive MDZ or DZP (Supasai et al., 2020). Both the piriform cortex and thalamus are thought to be sites for seizure initiation and subsequent injury (Bertram et al., 2008; Li et al., 2014; Myhrer et al., 2010) due to their oscillatory circuitry within the limbic system (reviewed in Vaughan and Jackson, 2014) or cerebral cortex (reviewed in Avanzini et al., 2000), respectively. The inability of MDZ and DZP to protect these regions highlights the need for novel antiseizure or neuroprotective therapies that can be applied after realistic delays between acutely intoxicating exposures to OPs and access to medical intervention.

In general, there were no significant differences in the efficacy of MDZ and DZP in attenuating neuropathology and neuroinflammation as detected by MRI or TSPO PET, respectively. However, there were several exceptions to this general conclusion. DFP animals treated with MDZ displayed significantly reduced neuroinflammation by TSPO PET in the inner layers of the cerebral cortex at 3 d post-exposure relative to DFP + DZP animals. Additionally, MDZ intervention significantly reduced DFP-induced neuroinflammation in the inner and outer cerebral cortex more consistently than DZP when each was compared to DFP animals that received no benzodiazepine intervention. Histological analyses of the brains from these animals similarly indicated that MDZ attenuated reactive astrogliosis more consistently across brain regions than DZP when assessed by GFAP and S100β immunoreactivity (Supasai et al., 2020). Neither MDZ nor DZP are known for their anti-inflammatory properties, although there are reports suggesting subtle immunomodulatory actions (reviewed in Cruz et al., 2017). These differences between MDZ and DZP with respect to attenuating neuroinflammation may reflect the fact that DFP + MDZ animals exhibited a trend towards lower average seizure severity scores compared to the DFP + DZP animals, suggesting improved seizure control with MDZ. However, this difference was not statistically significant (Supasai et al., 2020).

4.8. Seizure severity plays a role in later injury

We observed a significant positive correlation between the severity of seizure behavior in the initial hours following DFP intoxication and the severity of neuropathology and neuroinflammation as quantified by MRI and TPSO PET metrics. This association is a consistent finding across previous histological, behavioral, and imaging work in preclinical models of acute intoxication with DFP and other OPs (Carpentier et al., 2001; Hobson et al. 2017a, 2019; Prager et al., 2013; Siso et al., 2017). The strong association between the intensity or duration of seizures and subsequent injury supports the idea that single, high-dose injections of OPs predominantly mediate injury through induction of SE; however, animals with low seizure severity continue to exhibit neuropathology (Gonzalez et al., 2020). The benzodiazepines, MDZ and DZP, have potent antiseizure activity mediated by positive allosteric modulation of $GABA_A$ receptors (reviewed in Reddy and Reddy, 2015), and a significant reduction in seizure severity was observed following their application (Gonzalez et al., 2020). However, by nearly all imaging metrics reported here, and many histological assessments in these same animals (Supasai et al., 2020), neither benzodiazepine sufficiently mitigated neuropathology or neuroinflammation when administered at delayed times following DFP intoxication. Collectively, these data suggest that terminating seizures is the most crucial step following acute OP intoxication; however, antiseizure therapy must be supported by additional treatment options for addressing seizure-independent mechanisms.

5. Conclusions

This longitudinal study employing T2w and diffusion MRI, as well as TSPO PET, demonstrated progressive and persistent atrophy, neuropathology and neuroinflammation across multiple limbic and cortical areas in the rat brain during the 6 months following acute DFP intoxication. The relationship between early readouts of neuropathology and neuroinflammation and later brain atrophy were mixed, suggesting that multiple mechanisms may drive long-term outcomes. Administration of MDZ or DZP 40 min post-intoxication – a timeline emulating medical intervention in human OP intoxication scenarios – was variably effective in reducing brain atrophy and diffusion MRI indices of neuropathology depending on brain region. Neuroinflammation following DFP intoxication was largely resistant to attenuation by MDZ or DZP outside of the cerebral cortex. Critically, across all measures, neither benzodiazepine was reliably efficacious across all brain regions. In particular, the thalamus, which was severely damaged following acute DFP intoxication, was largely unaffected by benzodiazepine intervention. Collectively, these findings further highlight the limitations of current standard of care for treating acute OP intoxication and suggest attenuation of chronic neuroinflammation as a particularly promising therapeutic strategy to pursue. Finally, and perhaps related to inflammatory processes, the edematous lesions and microstructural changes observed on T2w and diffusion MRI are highly suggestive of dysfunctional regulation of fluid flow within the brain that would implicate disruption of the blood brain barrier as a candidate mechanism of injury and under-investigated therapeutic target.

Funding

This work was supported by the CounterACT Program, National Institutes of Health Office of the Director and the National Institute of Neurological Disorders and Stroke (U54 NS079202 and U54 NS127758 to P.J.L.), the National Institute of General Medical Sciences (T32 GM099608 to B.A.H.), the David and Dana Loury Foundation (predoctoral fellowship to B.A.H.), and the ARCS Foundation (predoctoral fellowship to B.A.H.). The sponsors were not involved in the study design, the collection, analysis, and interpretation of data, in the writing of the report or in the decision to submit the paper for publication.

CRediT authorship contribution statement

Brad A. Hobson: Writing – review & editing, Writing – original draft, Visualization, Validation, Methodology, Investigation, Formal analysis, Data curation, Conceptualization. **Douglas J. Rowland:** Visualization, Methodology, Investigation, Formal analysis, Data curation, Conceptualization. **Yimeng Dou:** Methodology, Investigation, Data curation. **Naomi Saito:** Visualization, Formal analysis. **Zachary T. Harmany:** Investigation, Formal analysis, Data curation. **Donald A. Bruun:** Writing – review & editing, Project administration, Investigation. **Danielle J. Harvey:** Writing – review & editing, Writing – original draft, Visualization, Formal analysis, Data curation. **Abhijit J. Chaudhari:** Writing – review & editing, Project administration. **Joel R. Garbow:** Writing – review & editing, Methodology, Conceptualization. **Pamela J. Lein:** Writing – review & editing, Supervision, Project administration, Funding acquisition, Conceptualization.

Declaration of competing interest

The authors declare the following financial interests/personal relationships which may be considered as potential competing interests:

Pamela J Lein reports financial support was provided by the National Institute of Neurological Disorders and Stroke CounterACT program. Brad A. Hobson reports financial support was provided by a T32 training program awarded to the University of California, Davis by the National Institute of General Medical Sciences and by a scholarship from the ARCS Foundation of Northern California.

Data availability

Data will be made available on request.

Acknowledgments

The authors gratefully thank Jennifer Fung and Charles Smith (UC Davis Center for Molecular and Genomic Imaging) for their assistance with animal care and imaging, Dave Kukis and Lina Planutyte (UC Davis Center for Molecular and Genomic Imaging) for assistance with radiotracer synthesis, Suren Bandara (UC Davis) for assistance with segmentation of MR images, and Dr. Simon Cherry (UC Davis) for advice on experimental design. The authors also thank Dr. Andrew Katsifis (Royal Prince Alfred Hospital, Sydney, Australia) for kindly providing precursor and standard material for the synthesis of [^{18}F]PBR111.

Appendix A. Supplementary data

Supplementary data to this article can be found online at https://doi.org/10.1016/j.neuropharm.2024.109918.

References

Abdel-Rahman, A., Shetty, A.K., Abou-Donia, M.B., 2002. Acute exposure to sarin increases blood brain barrier permeability and induces neuropathological changes in the rat brain: dose-response relationships. Neuroscience 113, 721–741.
Ackerman, J.J., Neil, J.J., 2010. The use of MR-detectable reporter molecules and ions to evaluate diffusion in normal and ischemic brain. NMR Biomed. 23, 725–733.
Altay, O., Suzuki, H., Hasegawa, Y., Ostrowski, R.P., Tang, J., Zhang, J.H., 2014. Isoflurane on brain inflammation. Neurobiol. Dis. 62, 365–371.
Andrew, P.M., Lein, P.J., 2021. Neuroinflammation as a therapeutic target for mitigating the long-term consequences of acute organophosphate intoxication. Front. Pharmacol. 12, 674325.
Apland, J.P., Aroniadou-Anderjaska, V., Figueiredo, T.H., Rossetti, F., Miller, S.L., Braga, M.F., 2014. The limitations of diazepam as a treatment for nerve agent-induced seizures and neuropathology in rats: comparison with UBP302. J Pharmacol Exp Ther 351, 359–372.
Arca, V., Marshall, S., Lake, W., Fedele, P., 2020. Guidelines for mass casualty decontamination during a terrorist chemical agent incident. US Army Soldier and Biological Chemical Command (SBCCOM) 1–56.
Aroniadou-Anderjaska, V., Figueiredo, T.H., Apland, J.P., Prager, E.M., Pidoplichko, V.I., Miller, S.L., Braga, M.F., 2016. Long-term neuropathological and behavioral impairments after exposure to nerve agents. Ann. N. Y. Acad. Sci. 1374, 17–28.
Avanzini, G., Panzica, F., de Curtis, M., 2000. The role of the thalamus in vigilance and epileptogenic mechanisms. Clin. Neurophysiol. 111 (Suppl. 2), S19–S26.
Baille, V., Clarke, P.G., Brochier, G., Dorandeu, F., Verna, J.M., Four, E., Lallement, G., Carpentier, P., 2005. Soman-induced convulsions: the neuropathology revisited. Toxicology 215, 1–24.
Banks, C.N., Lein, P.J., 2012. A review of experimental evidence linking neurotoxic organophosphorus compounds and inflammation. Neurotoxicology 33, 575–584.
Bar-Klein, G., Klee, R., Brandt, C., Bankstahl, M., Bascunana, P., Tollner, K., Dalipaj, H., Bankstahl, J.P., Friedman, A., Loscher, W., 2016. Isoflurane prevents acquired epilepsy in rat models of temporal lobe epilepsy. Ann. Neurol. 80, 896–908.
Bar-Klein, G., Lublinsky, S., Kamintsky, L., Noyman, I., Veksler, R., Dalipaj, H., Senatorov Jr., V.V., Swissa, E., Rosenbach, D., Elazary, N., Milikovsky, D.Z., Milk, N., Kassirer, M., Rosman, Y., Serlin, Y., Eisenkraft, A., Chassidim, Y., Parmet, Y., Kaufer, D., Friedman, A., 2017. Imaging blood-brain barrier dysfunction as a biomarker for epileptogenesis. Brain 140, 1692–1705.
Benjamini, Y., Hochberg, Y., 1995. Controlling the False Discovery rate: a Practical and powerful approach to multiple testing. J. Roy. Stat. Soc. B 57, 289–300.
Bernardino, P.N., Hobson, B.A., Huddleston, S.L., Andrew, P.M., MacMahon, J.A., Saito, N.H., Porter, V.A., Bruun, D.A., Harvey, D.J., Garbow, J.R., Gelli, A., Chaudhari, A.J., Lein, P.J., 2023a. Time- and region-dependent blood-brain barrier impairment in a rat model of organophosphate-induced status epilepticus. Neurobiol. Dis. 187, 106316.
Bernardino, P.N., Luo, A.S., Andrew, P.M., Unkel, C.M., Gonzalez, M.I., Gelli, A., Lein, P. J., 2023b. Evidence implicating blood-brain barrier impairment in the pathogenesis of acquired epilepsy following acute organophosphate intoxication. J Pharmacol Exp Ther.
Bernhardt, B.C., Worsley, K.J., Kim, H., Evans, A.C., Bernasconi, A., Bernasconi, N., 2009. Longitudinal and cross-sectional analysis of atrophy in pharmacoresistant temporal lobe epilepsy. Neurology 72, 1747–1754.
Bertoglio, D., Verhaeghe, J., Dedeurwaerdere, S., Grohn, O., 2017. Neuroimaging in animal models of epilepsy. Neuroscience 358, 277–299.
Bertram, E.H., Zhang, D., Williamson, J.M., 2008. Multiple roles of midline dorsal thalamic nuclei in induction and spread of limbic seizures. Epilepsia 49, 256–268.
Bhagat, Y.A., Obenaus, A., Hamilton, M.G., Kendall, E.J., 2001. Magnetic resonance imaging predicts neuropathology from soman-mediated seizures in the rodent. Neuroreport 12, 1481–1487.
Bhagat, Y.A., Obenaus, A., Hamilton, M.G., Mikler, J., Kendall, E.J., 2005. Neuroprotection from soman-induced seizures in the rodent: evaluation with diffusion- and T2-weighted magnetic resonance imaging. Neurotoxicology 26, 1001–1013.
Blair, R.E., Hawkins, E., Pinchbeck, L.R., DeLorenzo, R.J., Deshpande, L.S., 2024. Chronic epilepsy and Mossy fiber sprouting following organophosphate-induced status epilepticus in rats. J Pharmacol Exp Ther 388, 325–332.
Blumenfeld, H., 2007. Functional MRI studies of animal models in epilepsy. Epilepsia 48 (Suppl. 4), 18–26.
Bourdier, T., Pham, T.Q., Henderson, D., Jackson, T., Lam, P., Izard, M., Katsifis, A., 2012. Automated radiosynthesis of [18F]PBR102 using teh Tracerlab FXFN and Tracerlab MXFDG module for imaging the peripheral benzodiazepine receptor with PET. App. Radiat Isot 70, 176–183.
Brewer, K.L., Troendle, M.M., Pekman, L., Meggs, W.J., 2013. Naltrexone prevents delayed encephalopathy in rats poisoned with the sarin analogue diisopropylflurophosphate. Am. J. Emerg. Med. 31, 676–679.
Brigo, F., Nardone, R., Tezzon, F., Trinka, E., 2015. Nonintravenous midazolam versus intravenous or rectal diazepam for the treatment of early status epilepticus: a systematic review with meta-analysis. Epilepsy Behav. 49, 325–336.
Brooks, J., Erickson, T.B., Kayden, S., Ruiz, R., Wilkinson, S., Burkle, F.M., Jr, 2018. Responding to chemical weapons violations in Syria: legal, health, and humanitarian recommendations. Confl Health 12, 12.
Bruun, D.A., Guignet, M., Harvey, D.J., Lein, P.J., 2019. Pretreatment with pyridostigmine bromide has no effect on seizure behavior or 24 hour survival in the rat model of acute diisopropylfluorophosphate intoxication. Neurotoxicology 73, 81–84.
Budde, M.D., Skinner, N.P., 2018. Diffusion MRI in acute nervous system injury. J. Magn. Reson. 292, 137–148.
Carpentier, P., Foquin, A., Kamenka, J.M., Rondouin, G., Lerner-Natoli, M., de Groot, D. M., Lallement, G., 2001. Effects of thienylphencyclidine (TCP) on seizure activity and brain damage produced by soman in Guinea-pigs: ECoG correlates of neurotoxicity. Neurotoxicology 22, 13–28.
Carpentier, P., Testylier, G., Dorandeu, F., Segebarth, C., Montigon, O., Foquin, A., Lahrech, H., 2008. Hyperosmolar treatment of soman-induced brain lesions in mice: evaluation of the effects through diffusion-weighted magnetic resonance imaging and through histology. Toxicology 253, 97–103.
Chen, Y., 2012. Organophosphate-induced brain damage: mechanisms, neuropsychiatric and neurological consequences, and potential therapeutic strategies. Neurotoxicology 33, 391–400.
Collombet, J.M., 2011. Nerve agent intoxication: recent neuropathophysiological findings and subsequent impact on medical management prospects. Toxicol. Appl. Pharmacol. 255, 229–241.
Cowan, F.M., Broomfield, C.A., Lenz, D.E., Smith, W.J., 2003. Putative role of proteolysis and inflammatory response in the toxicity of nerve and blister chemical warfare agents: implications for multi-threat medical countermeasures. J. Appl. Toxicol. 23, 177–186.
Cruz, F.F., Rocco, P.R., Pelosi, P., 2017. Anti-inflammatory properties of anesthetic agents. Crit. Care 21, 67.
de Araujo Furtado, M., Lumley, L.A., Robison, C., Tong, L.C., Lichtenstein, S., Yourick, D. L., 2010. Spontaneous recurrent seizures after status epilepticus induced by soman in Sprague-Dawley rats. Epilepsia 51, 1503–1510.
Deshpande, L.S., Carter, D.S., Blair, R.E., DeLorenzo, R.J., 2010. Development of a prolonged calcium plateau in hippocampal neurons in rats surviving status epilepticus induced by the organophosphate diisopropylfluorophosphate. Toxicol. Sci. 116, 623–631.
Dietrich, Y., Eliat, P.A., Dieuset, G., Saint-Jalmes, H., Pineau, C., Wendling, F., Martin, B., 2016. Structural and functional changes during epileptogenesis in the mouse model of medial temporal lobe epilepsy. Conf Proc IEEE Eng Med Biol Soc. 2016, 4005–4008.
Dreier, J.P., Lemale, C.L., Kola, V., Friedman, A., Schoknecht, K., 2018. Spreading depolarization is not an epiphenomenon but the principal mechanism of the cytotoxic edema in various gray matter structures of the brain during stroke. Neuropharmacology 134, 189–207.
Eddleston, M., Buckley, N.A., Eyer, P., Dawson, A.H., 2008. Management of acute organophosphorus pesticide poisoning. Lancet 371, 597–607.
FDA. Center For Drug Evaluation and Research - Midazolam Review, 2018. In: Food and Drug Administration. Application 209566Orig1s000.
Figueiredo, T.H., Apland, J.P., Braga, M.F.M., Marini, A.M., 2018. Acute and long-term consequences of exposure to organophosphate nerve agents in humans. Epilepsia 59 (Suppl. 2), 92–99.
Flannery, B.M., Bruun, D.A., Rowland, D.J., Banks, C.N., Austin, A.T., Kukis, D.L., Li, Y., Ford, B.D., Tancredi, D.J., Silverman, J.L., Cherry, S.R., Lein, P.J., 2016. Persistent neuroinflammation and cognitive impairment in a rat model of acute diisopropylfluorophosphate intoxication. J. Neuroinflammation 13, 267.
Gage, M., Rao, N.S., Samidurai, M., Putra, M., Vasanthi, S.S., Meyer, C., Wang, C., Thippeswamy, T., 2021. Soman (GD) rat model to Mimic civilian exposure to nerve agent: mortality, Video-EEG based status epilepticus severity, Sex differences, spontaneously recurring seizures, and brain pathology. Front. Cell. Neurosci. 15, 798247.
Gao, J., Naughton, S.X., Wulff, H., Singh, V., Beck, W.D., Magrane, J., Thomas, B., Kaidery, N.A., Hernandez, C.M., Terry Jr., A.V., 2016. Diisopropylfluorophosphate impairs the transport of Membrane-Bound Organelles in rat cortical Axons. J Pharmacol Exp Ther 356, 645–655.
Gonzalez, E.A., Rindy, A.C., Guignet, M.A., Calsbeek, J.J., Bruun, D.A., Dhir, A., Andrew, P., Saito, N., Rowland, D.J., Harvey, D.J., Rogawski, M.A., Lein, P.J., 2020. The chemical convulsant diisopropylfluorophosphate (DFP) causes persistent neuropathology in adult male rats independent of seizure activity. Arch. Toxicol. 94, 2149–2162.
Grohn, O., Pitkanen, A., 2007. Magnetic resonance imaging in animal models of epilepsy-noninvasive detection of structural alterations. Epilepsia 48 (Suppl. 4), 3–10.

Guignet, M., Dhakal, K., Flannery, B.M., Hobson, B.A., Zolkowska, D., Dhir, A., Bruun, D. A., Li, S., Wahab, A., Harvey, D.J., Silverman, J.L., Rogawski, M.A., Lein, P.J., 2020. Persistent behavior deficits, neuroinflammation, and oxidative stress in a rat model of acute organophosphate intoxication. Neurobiol. Dis. 133, 104431.
Gullapalli, R.P., Aracava, Y., Zhuo, J., Helal Neto, E., Wang, J., Makris, G., Merchenthaler, I., Pereira, E.F., Albuquerque, E.X., 2010. Magnetic resonance imaging reveals that galantamine prevents structural brain damage induced by an acute exposure of Guinea pigs to soman. Neurotoxicology 31, 67–76.
Gupta, A., Agarwal, R., Shukla, G.S., 1999. Functional impairment of blood-brain barrier following pesticide exposure during early development in rats. Hum. Exp. Toxicol. 18, 174–179.
Hartings, J.A., Shuttleworth, C.W., Kirov, S.A., Ayata, C., Hinzman, J.M., Foreman, B., Andrew, R.D., Boutelle, M.G., Brennan, K.C., Carlson, A.P., Dahlem, M.A., Drenckhahn, C., Dohmen, C., Fabricius, M., Farkas, E., Feuerstein, D., Graf, R., Helbok, R., Lauritzen, M., Major, S., Oliveira-Ferreira, A.I., Richter, F., Rosenthal, E. S., Sakowitz, O.W., Sanchez-Porras, R., Santos, E., Scholl, M., Strong, A.J., Urbach, A., Westover, M.B., Winkler, M.K., Witte, O.W., Woitzik, J., Dreier, J.P., 2017. The continuum of spreading depolarizations in acute cortical lesion development: Examining Leao's legacy. J Cereb Blood Flow Metab 37, 1571–1594.
Heemskerk, J.L., Abode-Iyamah, K.O., Quinones-Hinojosa, A., Weinstein, E.S., 2022. Prehospital response time of the Emergency medical Service during mass casualty Incidents and the effect of triage: a Retrospective study. Disaster Med. Public Health Prep. 16, 1091–1098.
Hill, C.E., Parikh, A.O., Ellis, C., Myers, J.S., Litt, B., 2017. Timing is everything: where status epilepticus treatment fails. Ann. Neurol. 82, 155–165.
Hobson, B.A., Rowland, D.J., Siso, S., Guignet, M.A., Harmany, Z.T., Bandara, S.B., Saito, N., Harvey, D.J., Bruun, D.A., Garbow, J.R., Chaudhari, A.J., Lein, P.J., 2019. TSPO PET using [18F]PBR111 reveals persistent neuroinflammation following acute diisopropylfluorophosphate intoxication in the rat. Toxicol. Sci. 170, 330–344.
Hobson, B.A., Rowland, D.J., Supasai, S., Harvey, D.J., Lein, P.J., Garbow, J.R., 2017a. A magnetic resonance imaging study of early brain injury in a rat model of acute DFP intoxication. Neurotoxicology.
Hobson, B.A., Siso, S., Rowland, D.J., Harvey, D.J., Bruun, D.A., Garbow, J.R., Lein, P.J., 2017b. Magnetic resonance imaging reveals progressive brain injury in rats acutely intoxicated with diisopropylfluorophosphate. Toxicol. Sci. 157, 342–353.
Hrabe, J., Kaur, G., Guilfoyle, D.N., 2007. Principles and limitations of NMR diffusion measurements. J. Med. Phys. 32, 34–42.
Hubers, A., Thoma, K., Schocke, M., Fauser, S., Ludolph, A.C., Kassubek, J., Pinkhardt, E. H., 2018. Acute DWI reductions in patients after single epileptic seizures - more common than assumed. Front. Neurol. 9, 550.
Jett, D.A., Sibrizzi, C.A., Blain, R.B., Hartman, P.A., Lein, P.J., Taylor, K.W., Rooney, A. A., 2020. A national toxicology program systematic review of the evidence for long-term effects after acute exposure to sarin nerve agent. Crit. Rev. Toxicol. 50, 474–490.
Jones, T.A., Bury, S.D., Adkins-Muir, D.L., Luke, L.M., Allred, R.P., Sakata, J.T., 2003. Importance of behavioral manipulations and measures in rat models of brain damage and brain repair. ILAR J. 44, 144–152.
Jupp, B., Williams, J., Binns, D., Hicks, R.J., Cardamone, L., Jones, N., Rees, S., O'Brien, T.J., 2012. Hypometabolism precedes limbic atrophy and spontaneous recurrent seizures in a rat model of TLE. Epilepsia 53, 1233–1244.
Kapur, J., Elm, J., Chamberlain, J.M., Barsan, W., Cloyd, J., Lowenstein, D., Shinnar, S., Conwit, R., Meinzer, C., Cock, H., Fountain, N., Connor, J.T., Silbergleit, R., Nett, InvestigatorsP, 2019. Randomized trial of three anticonvulsant Medications for status epilepticus. N. Engl. J. Med. 381, 2103–2113.
Kharatishvili, I., Shan, Z.Y., She, D.T., Foong, S., Kurniawan, N.D., Reutens, D.C., 2014. MRI changes and complement activation correlate with epileptogenicity in a mouse model of temporal lobe epilepsy. Brain Struct. Funct. 219, 683–706.
Kim, J., Kim, C.H., Shin, S.D., Park, J.O., 2018. Prehospital response time delays for Emergency patients in events of concurrent mass casualty Incidents. Disaster Med. Public Health Prep. 12, 94–100.
Kirschenbaum, L., Keene, A., O'Neill, P., Westfal, R., Astiz, M.E., 2005. The experience at St. Vincent's Hospital, Manhattan, on September 11, 2001: preparedness, response, and lessons learned. Crit. Care Med. 33, S48–S52.
Krutak-Krol, H., Domino, E.F., 1985. Comparative effects of diazepam and midazolam on paraoxon toxicity in rats. Toxicol. Appl. Pharmacol. 81, 545–550.
Kuroiwa, T., Miyasaka, N., Fengyo, Z., Yamada, I., Nakane, M., Nagaoka, T., Tamura, A., Ohno, K., 2007. Experimental ischemic brain edema: morphological and magnetic resonance imaging findings. Neurosurg. Focus 22, E11.
Kuruba, R., Wu, X., Reddy, D.S., 2018. Benzodiazepine-refractory status epilepticus, neuroinflammation, and interneuron neurodegeneration after acute organophosphate intoxication. Biochim. Biophys. Acta 1864, 2845–2858.
Lallement, G., Clarencon, D., Masqueliez, C., Baubichon, D., Galonnier, M., Burckhart, M. F., Peoc'h, M., Mestries, J.C., 1998. Nerve agent poisoning in primates: antilethal, anti-epileptic and neuroprotective effects of GK-11. Arch. Toxicol. 72, 84–92.
Langner, S., Fleck, S., Baldauf, J., Mensel, B., Kuhn, J.P., Kirsch, M., 2017. Diagnosis and differential Diagnosis of hydrocephalus in adults. Röfo 189, 728–739.
Leinonen, V., Vanninen, R., Rauramaa, T., 2017. Cerebrospinal fluid circulation and hydrocephalus. Handb. Clin. Neurol. 145, 39–50.
Li, F., Liu, K.F., Silva, M.D., Omae, T., Sotak, C.H., Fenstermacher, J.D., Fisher, M., Hsu, C.Y., Lin, W., 2000. Transient and permanent resolution of ischemic lesions on diffusion-weighted imaging after brief periods of focal ischemia in rats : correlation with histopathology. Stroke 31, 946–954.
Li, Y.H., Li, J.J., Lu, Q.C., Gong, H.Q., Liang, P.J., Zhang, P.M., 2014. Involvement of thalamus in initiation of epileptic seizures induced by pilocarpine in mice. Neural Plast. 2014, 675128.
McDonough Jr., J.H., McMonagle, J., Copeland, T., Zoeffel, D., Shih, T.M., 1999. Comparative evaluation of benzodiazepines for control of soman-induced seizures. Arch. Toxicol. 73, 473–478.
McDonough Jr., J.H., Shih, T.M., 1997. Neuropharmacological mechanisms of nerve agent-induced seizure and neuropathology. Neurosci. Biobehav. Rev. 21, 559–579.
McDonough, J.H., McMonagle, J.D., Shih, T.M., 2010. Time-dependent reduction in the anticonvulsant effectiveness of diazepam against soman-induced seizures in Guinea pigs. Drug Chem. Toxicol. 33, 279–283.
McMullan, J., Sasson, C., Pancioli, A., Silbergleit, R., 2010. Midazolam versus diazepam for the treatment of status epilepticus in children and young adults: a meta-analysis. Acad. Emerg. Med. 17, 575–582.
Mew, E.J., Padmanathan, P., Konradsen, F., Eddleston, M., Chang, S.S., Phillips, M.R., Gunnell, D., 2017. The global burden of fatal self-poisoning with pesticides 2006-15: systematic review. J. Affect. Disord. 219, 93–104.
Michinaga, S., Koyama, Y., 2015. Pathogenesis of brain edema and investigation into anti-edema drugs. Int. J. Mol. Sci. 16, 9949–9975.
Myhrer, T., Enger, S., Aas, P., 2010. Roles of perirhinal and posterior piriform cortices in control and generation of seizures: a microinfusion study in rats exposed to soman. Neurotoxicology 31, 147–153.
Nair, A.B., Jacob, S., 2016. A simple practice guide for dose conversion between animals and human. J. Basic Clin. Pharm. 7, 27–31.
Newmark, J., 2004. Nerve agents: pathophysiology and treatment of poisoning. Semin. Neurol. 24, 185–196.
Newmark, J., 2019. Therapy for acute nerve agent poisoning: an update. Neurol Clin Pract 9, 337–342.
Obenaus, A., Jacobs, R.E., 2007. Magnetic resonance imaging of functional anatomy: use for small animal epilepsy models. Epilepsia 48 (Suppl. 4), 11–17.
Paxinos, G., Watson, C., 2007. The Rat Brain in Stereotaxic Coordinates, sixth ed. Academic Press/Elsevier, Amsterdam ; Boston.
Pereira, E.F., Aracava, Y., DeTolla Jr., L.J., Beecham, E.J., Basinger Jr., G.W., Wakayama, E.J., Albuquerque, E.X., 2014. Animal models that best reproduce the clinical manifestations of human intoxication with organophosphorus compounds. J Pharmacol Exp Ther 350, 313–321.
Pfenninger, E.G., Klingler, W., Keiloweit, T., Eble, M., Wenzel, V., Kruger, W.A., 2020. [Terrorist attack training exercise-What can be learned? : Baden-Wurttemberg counterterrorism exercise (BWTEX)]. Anaesthesist 69, 477–486.
Polli, R.S., Malheiros, J.M., Dos Santos, R., Hamani, C., Longo, B.M., Tannus, A., Mello, L. E., Covolan, L., 2014. Changes in hippocampal volume are correlated with cell loss but not with seizure frequency in two chronic models of temporal lobe epilepsy. Front. Neurol. 5, 111.
Pouliot, W., Bealer, S.L., Roach, B., Dudek, F.E., 2016. A rodent model of human organophosphate exposure producing status epilepticus and neuropathology. Neurotoxicology 56, 196–203.
Power, S., Symons, C., Carter, H., Jones, E., Amlot, R., Larner, J., Matar, H., Chilcott, R. P., 2016. Mass casualty decontamination in the United States: an online Survey of current practice. Health Secur 14, 226–236.
Prager, E.M., Aroniadou-Anderjaska, V., Almeida-Suhett, C.P., Figueiredo, T.H., Apland, J.P., Braga, M.F., 2013. Acetylcholinesterase inhibition in the basolateral amygdala plays a key role in the induction of status epilepticus after soman exposure. Neurotoxicology 38, 84–90.
Raines, A., Henderson, T.R., Swinyard, E.A., Dretchen, K.L., 1990. Comparison of midazolam and diazepam by the intramuscular route for the control of seizures in a mouse model of status epilepticus. Epilepsia 31, 313–317.
Reddy, D.S., Zaayman, M., Kuruba, R., Wu, X., 2021. Comparative profile of refractory status epilepticus models following exposure of cholinergic agents pilocarpine, DFP, and soman. Neuropharmacology 191, 108571.
Reddy, S.D., Reddy, D.S., 2015. Midazolam as an anticonvulsant antidote for organophosphate intoxication–A pharmacotherapeutic appraisal. Epilepsia 56, 813–821.
Reddy, S.D., Wu, X., Kuruba, R., Sridhar, V., Reddy, D.S., 2020. Magnetic resonance imaging analysis of long-term neuropathology after exposure to the nerve agent soman: correlation with histopathology and neurological dysfunction. Ann. N. Y. Acad. Sci. 1480, 116–135.
Reddy, S.D., Younus, I., Sridhar, V., Reddy, D.S., 2019. Neuroimaging biomarkers of experimental epileptogenesis and refractory epilepsy. Int. J. Mol. Sci. 20.
Rennebaum, F., Kassubek, J., Pinkhardt, E., Hubers, A., Ludolph, A.C., Schocke, M., Fauser, S., 2016. Status epilepticus: clinical characteristics and EEG patterns associated with and without MRI diffusion restriction in 69 patients. Epilepsy Res. 120, 55–64.
Roch, C., Leroy, C., Nehlig, A., Namer, I.J., 2002. Predictive value of cortical injury for the development of temporal lobe epilepsy in 21-day-old rats: an MRI approach using the lithium-pilocarpine model. Epilepsia 43, 1129–1136.
Rojas, A., Abreu-Melon, J., Wang, S., Dingledine, R., 2022. Time-dependent neuropathology in rats following organophosphate-induced status epilepticus. Neurotoxicology 91, 45–59.
Rojas, A., Ganesh, T., Lelutiu, N., Gueorguieva, P., Dingledine, R., 2015. Inhibition of the prostaglandin EP2 receptor is neuroprotective and accelerates functional recovery in a rat model of organophosphorus induced status epilepticus. Neuropharmacology 93, 15–27.
Rosman, Y., Eisenkraft, A., Krivoy, A., Schein, O., Makarovski, I., Shrot, S., Ramaty, E., Shilderman, E.B., Kapon, J., Gilat, E., Kadar, T., Maier, S., Daniels, D., Shneor, R., Salomon, S., Tamar, G., Last, D., Mardor, Y., 2012. Using MRI for the assessment of paraoxon-induced brain damage and efficacy of antidotal treatment. J. Appl. Toxicol. 32, 409–416.
Salo, R.A., Miettinen, T., Laitinen, T., Grohn, O., Sierra, A., 2017. Diffusion tensor MRI shows progressive changes in the hippocampus and dentate gyrus after status

epilepticus in rat - histological validation with Fourier-based analysis. Neuroimage 152, 221–236.
Savage, E.P., Keefe, T.J., Mounce, L.M., Heaton, R.K., Lewis, J.A., Burcar, P.J., 1988. Chronic neurological sequelae of acute organophosphate pesticide poisoning. Arch. Environ. Health 43, 38–45.
Schindelin, J., Arganda-Carreras, I., Frise, E., Kaynig, V., Longair, M., Pietzsch, T., Preibisch, S., Rueden, C., Saalfeld, S., Schmid, B., Tinevez, J.Y., White, D.J., Hartenstein, V., Eliceiri, K., Tomancak, P., Cardona, A., 2012. Fiji: an open-source platform for biological-image analysis. Nat. Methods 9, 676–682.
Schober, P., Boer, C., Schwarte, L.A., 2018. Correlation coefficients: Appropriate Use and interpretation. Anesth. Analg. 126, 1763–1768.
Scholl, E.A., Miller-Smith, S.M., Bealer, S.L., Lehmkuhle, M.J., Ekstrand, J.J., Dudek, F. E., McDonough, J.H., 2018. Age-dependent behaviors, seizure severity and neuronal damage in response to nerve agents or the organophosphate DFP in immature and adult rats. Neurotoxicology 66, 10–21.
Shih, T., McDonough Jr., J.H., Koplovitz, I., 1999. Anticonvulsants for soman-induced seizure activity. J. Biomed. Sci. 6, 86–96.
Shih, T.M., Duniho, S.M., McDonough, J.H., 2003. Control of nerve agent-induced seizures is critical for neuroprotection and survival. Toxicol. Appl. Pharmacol. 188, 69–80.
Shrot, S., Anaby, D., Krivoy, A., Makarovsky, I., Rosman, Y., Bloch-Shilderman, E., Lazar, S., Bar-Shir, A., Cohen, Y., 2012. Early in vivo MR spectroscopy findings in organophosphate-induced brain damage-potential biomarkers for short-term survival. Magn. Reson. Med. 68, 1390–1398.
Shrot, S., Tauber, M., Shiyovich, A., Milk, N., Rosman, Y., Eisenkraft, A., Kadar, T., Kassirer, M., Cohen, Y., 2015. Early brain magnetic resonance imaging can predict short and long-term outcomes after organophosphate poisoning in a rat model. Neurotoxicology 48, 206–216.
Silbergleit, R., Lowenstein, D., Durkalski, V., Conwit, R., Neurological Emergency Treatment Trials I, 2011. RAMPART (Rapid Anticonvulsant Medication Prior to Arrival Trial): a double-blind randomized clinical trial of the efficacy of intramuscular midazolam versus intravenous lorazepam in the prehospital treatment of status epilepticus by paramedics. Epilepsia 52 (Suppl. 8), 45–47.
Siso, S., Hobson, B.A., Harvey, D.J., Bruun, D.A., Rowland, D.J., Garbow, J.R., Lein, P.J., 2017. Spatiotemporal progression and Remission of lesions in the rat brain following acute intoxication with diisopropylfluorophosphate. Toxicol. Sci. 157, 330–341.
Song, X., Pope, C., Murthy, R., Shaikh, J., Lal, B., Bressler, J.P., 2004. Interactive effects of paraoxon and pyridostigmine on blood-brain barrier integrity and cholinergic toxicity. Toxicol. Sci. 78, 241–247.
Stuckey, S.M., Ong, L.K., Collins-Praino, L.E., Turner, R.J., 2021. Neuroinflammation as a key driver of secondary neurodegeneration following stroke? Int. J. Mol. Sci. 22.
Suleymanova, E., Gulyaev, M., Chepurnova, N., 2014. Ginseng extract attenuates early MRI changes after status epilepticus and decreases subsequent reduction of hippocampal volume in the rat brain. Epilepsy Res. 108, 223–231.
Supasai, S., Gonzalez, E.A., Rowland, D.J., Hobson, B., Bruun, D.A., Guignet, M.A., Soares, S., Singh, V., Wulff, H., Saito, N., Harvey, D.J., Lein, P.J., 2020. Acute administration of diazepam or midazolam minimally alters long-term neuropathological effects in the rat brain following acute intoxication with diisopropylfluorophosphate. Eur. J. Pharmacol. 886, 173538.
Swissa, E., Bar-Klein, G., Serlin, Y., Weissberg, I., Kamintsky, L., Eisenkraft, A., Statlender, L., Shrot, S., Rosman, Y., Prager, O., Friedman, A., 2020. Midazolam and isoflurane combination reduces late brain damage in the paraoxon-induced status epilepticus rat model. Neurotoxicology 78, 99–105.
Testylier, G., Lahrech, H., Montigon, O., Foquin, A., Delacour, C., Bernabe, D., Segebarth, C., Dorandeu, F., Carpentier, P., 2007. Cerebral edema induced in mice by a convulsive dose of soman. Evaluation through diffusion-weighted magnetic resonance imaging and histology. Toxicol. Appl. Pharmacol. 220, 125–137.
Tokumitsu, T., Mancuso, A., Weinstein, P.R., Weiner, M.W., Naruse, S., Maudsley, A.A., 1997. Metabolic and pathological effects of temporal lobe epilepsy in rat brain detected by proton spectroscopy and imaging. Brain Res. 744, 57–67.
Towne, A.R., 2007. Epidemiology and outcomes of status epilepticus in the elderly. Int. Rev. Neurobiol. 81, 111–127.
Ulu, A., Inceoglu, B., Yang, J., Singh, V., Vito, S., Wulff, H., Hammock, B.D., 2016. Inhibition of soluble epoxide hydrolase as a novel approach to high dose diazepam induced hypotension. J. Clin. Toxicol. 6.
Van Camp, N., Boisgard, R., Kuhnast, B., Theze, B., Viel, T., Gregoire, M.C., Chauveau, F., Boutin, H., Katsifis, A., Dolle, F., Tavitian, B., 2010. In vivo imaging of neuroinflammation: a comparative study between [(18)F]PBR111, [(11)C]CLINME and [(11)C]PK11195 in an acute rodent model. Eur J Nucl Med Mol Imaging 37, 962–972.
Van Camp, N., Lavisse, S., Roost, P., Gubinelli, F., Hillmer, A., Boutin, H., 2021. TSPO imaging in animal models of brain diseases. Eur J Nucl Med Mol Imaging 49, 77–109.
van Vliet, E.A., Otte, W.M., Wadman, W.J., Aronica, E., Kooij, G., de Vries, H.E., Dijkhuizen, R.M., Gorter, J.A., 2016. Blood-brain barrier leakage after status epilepticus in rapamycin-treated rats I: magnetic resonance imaging. Epilepsia 57, 59–69.
Vardell, E., 2012. Chemical Hazards Emergency medical management (CHEMM). Med. Ref. Serv. Q. 31, 73–83.
Vaughan, D.N., Jackson, G.D., 2014. The piriform cortex and human focal epilepsy. Front. Neurol. 5, 259.
Vezzani, A., Balosso, S., Ravizza, T., 2019. Neuroinflammatory pathways as treatment targets and biomarkers in epilepsy. Nat. Rev. Neurol. 15, 459–472.
Vossler, D.G., Bainbridge, J.L., Boggs, J.G., Novotny, E.J., Loddenkemper, T., Faught, E., Amengual-Gual, M., Fischer, S.N., Gloss, D.S., Olson, D.M., Towne, A.R., Naritoku, D., Welty, T.E., 2020. Treatment of refractory convulsive status epilepticus: a comprehensive review by the American epilepsy Society treatments Committee. Epilepsy Curr. 20, 245–264.
Werry, E.L., Bright, F.M., Piguet, O., Ittner, L.M., Halliday, G.M., Hodges, J.R., Kiernan, M.C., Loy, C.T., Kril, J.J., Kassiou, M., 2019. Recent developments in TSPO PET imaging as A biomarker of neuroinflammation in neurodegenerative Disorders. Int. J. Mol. Sci. 20.
Wu, X., Kuruba, R., Reddy, D.S., 2018a. Midazolam-resistant seizures and brain injury after acute intoxication of diisopropylfluorophosphate, an organophosphate pesticide and Surrogate for nerve agents. J Pharmacol Exp Ther 367, 302–321.
Wu, X., Kuruba, R., Reddy, D.S., 2018b. Midazolam-resistant seizures and brain injury following acute intoxication of diisopropylfluorophosphate, an organophosphate pesticide and Surrogate for nerve agents. J Pharmacol Exp Ther.
Yamasue, H., Abe, O., Kasai, K., Suga, M., Iwanami, A., Yamada, H., Tochigi, M., Ohtani, T., Rogers, M.A., Sasaki, T., Aoki, S., Kato, T., Kato, N., 2007. Human brain structural change related to acute single exposure to sarin. Ann. Neurol. 61, 37–46.
Yankam Njiwa, J., Costes, N., Bouillot, C., Bouvard, S., Fieux, S., Becker, G., Levigoureux, E., Kocevar, G., Stamile, C., Langlois, J.B., Bolbos, R., Bonnet, C., Bezin, L., Zimmer, L., Hammers, A., 2017. Quantitative longitudinal imaging of activated microglia as a marker of inflammation in the pilocarpine rat model of epilepsy using [(11)C]-(R)-PK11195 PET and MRI. J Cereb Blood Flow Metab 37, 1251–1263.
Yogarajah, M., Duncan, J.S., 2008. Diffusion-based magnetic resonance imaging and tractography in epilepsy. Epilepsia 49, 189–200.
Zimmer, L.A., Ennis, M., Shipley, M.T., 1997. Soman-induced seizures rapidly activate astrocytes and microglia in discrete brain regions. J. Comp. Neurol. 378, 482–492.